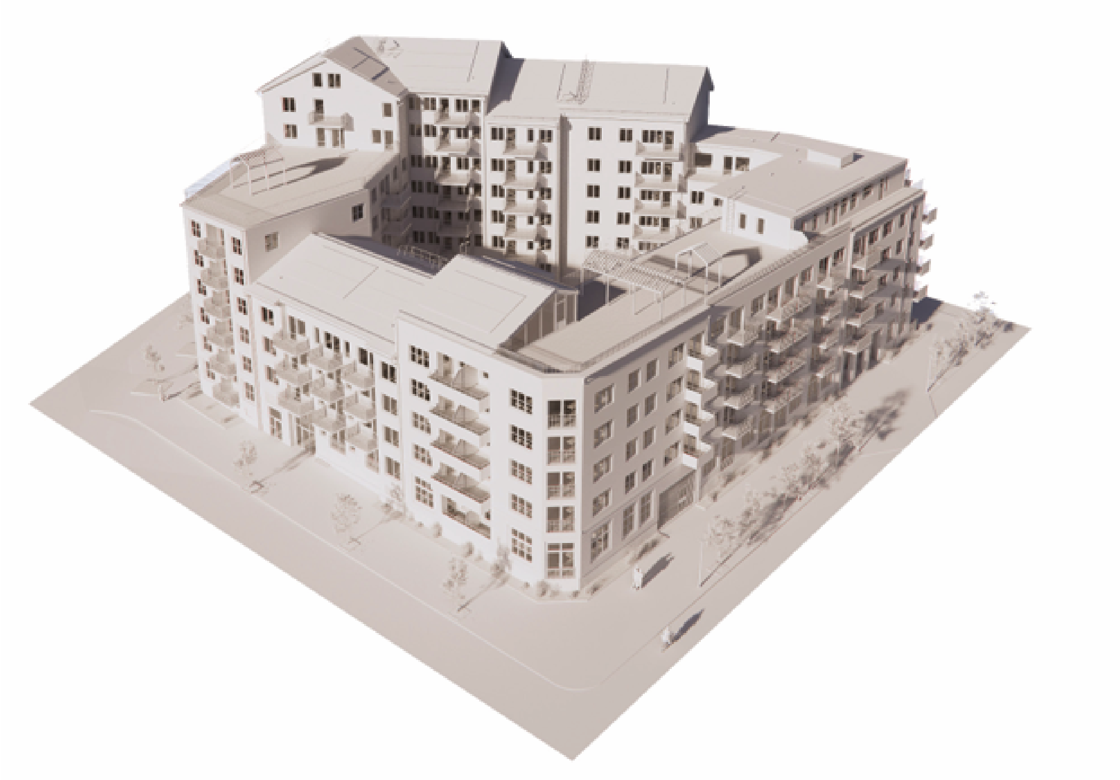

Evaluating 56-Day Strength as a Basis for Design in Climate-Reduced Concrete

Master's thesis in the Master's Programme Structural Engineering and Building Technology

SAGA SERNEKVIST

DEPARTMENT OF ARCHITECTURE AND CIVIL ENGINEERING
DIVISION OF STRUCTURAL ENGINEERING

CHALMERS UNIVERSITY OF TECHNOLOGY
Master's thesis ACEX30
Gothenburg, Sweden 2026

MASTER'S THESIS ACEX30

Evaluating 56-Day Strength as a Basis for Design in Climate-Reduced Concrete

Master's Thesis in the Master's Programme Structural Engineering and Building Technology

SAGA SERNEKVIST

Department of Architecture and Civil Engineering
Division of Structural engineering
CHALMERS UNIVERSITY OF TECHNOLOGY
Gothenburg, Sweden 2026

Evaluating 56-Day Strength as a Basis for Design in Climate-Reduced Concrete
Master's Thesis in the Master's Programme Structural Engineering and Building Technology

SAGA SERNEKVIST

Examiner: Carlos Gil Berrocal, Department of Architecture and Civil Engineering

Examensarbete ACEX30
Institutionen för Arkitektur och Samhällsbyggnadsteknik
Chalmers Tekniska Högskola, 2026

Department of Architecture and Civil Engineering
Division of Structural Engineering
Chalmers University of Technology
SE-412 96 Göteborg
Sweden
Telephone +46 31 772 1000

Cover:
Reference building used in the case study analysis.
Department of Architecture and Civil Engineering
Göteborg, Sweden, 2026

Evaluating 56-Day Strength as a Basis for Design in Climate-Reduced Concrete
Master's thesis in the Master's Programme Structural Engineering and Building Technology

Saga Sernekvist
Department of Architecture and Civil Engineering
Division of Structural Engineering
Chalmers University of Technology

ABSTRACT

The construction sector is responsible for a significant share of global greenhouse gas emissions, primarily due to the production of Portland cement. To address this, supplementary cementitious materials such as Ground Granulated Blast-furnace Slag (GGBS) are increasingly used as partial cement replacements in climate-reduced concrete. While these materials reduce embodied carbon, they also alter the strength development characteristics of the concrete, most notably by slowing early-age strength gain while enabling continued strength development beyond 28 days.

Current structural design practice evaluates concrete compressive strength at 28 days, which is the basis for concrete classification under Eurocode 2. For slag-containing concretes, this approach neglects a potentially significant additional strength gain at later ages. This thesis investigates whether 56-day compressive strength can serve as a viable basis for structural design, and evaluates the practical implications for strength development, reinforcement demand, and embodied carbon.

Laboratory data from concrete mixes with GGBS contents between 26% and 51% were analysed, showing relative strength increases between 28 and 56 days ranging from approximately 3% to 13%. A numerical strength development model was calibrated using in-situ temperature measurements from six floor slabs in a residential building constructed with 32% GGBS concrete. The calibrated model was applied to three structural elements, a filigree floor slab, a ground slab, and a basement external wall, using spring temperature data from Gothenburg as boundary conditions.

The results show that C28/35 concrete with 32% GGBS can approach or reach the 37 MPa cube strength associated with C30/37, but that all investigated elements required considerably longer than 56 days under the simulated conditions, with approximately 80 days being a more representative figure for this specific case. The reinforcement demand was governed by ULS bending for the floor slab, where concrete strength class has only a minor influence, and by crack width control for the ground slab and basement wall, where the difference between C28/35 and C30/37 amounts to 22 mm²/m.

A reduction in strength class from C30/37 to C28/35 is estimated to reduce total CO_2-equivalent emissions by approximately 6% at Level 3 and 4% at Level 4 climate performance. The study concludes that later-age strength development in GGBS concrete offers measurable potential for more efficient structural design, but that careful consideration of early-age behaviour, curing conditions, and production constraints is required before such an approach can be applied in practice.

Statement on the use of AI:

Artificial intelligence (AI) tools have been used to support the writing process, mainly for improving the readability and flow of the text, as well as assisting with formatting and table layout.

Key words:
Climate-reduced concrete, GGBS, Compressive strength, 56-day strength, Structural design, Maturity method, Embodied carbon

Utvärdering av 56-dygnshållfasthet som dimensioneringsgrund för klimatförbättrad betong
Examensarbete inom masterprogrammet konstruktionsteknik och byggnadsteknologi

SAGA SERNEKVIST

Institutionen för arkitektur och samhällsbyggnadsteknik
Avdelningen för Konstruktionsteknik
Chalmers tekniska högskola

SAMMANFATTNING

Byggsektorn står för en betydande andel av de globala växthusgasutsläppen, framför allt till följd av produktionen av portlandcement. Som svar på detta används supplementära cementösa material, såsom masugnsslagg (GGBS), i allt större utsträckning som delvisa ersättningar för cement i klimatförbättrad betong. Dessa material minskar byggnadens klimatpåverkan men förändrar även betongens hållfasthetsutveckling, framförallt genom att den tidiga hållfastheten uppnås långsammare, medan hållfastheten fortsätter att öka avsevärt efter 28 dygn.

Nuvarande dimensioneringspraxis utvärderar betongens tryckhållfasthet vid 28 dygn, vilket utgör grunden för klassificering enligt Eurokod 2. För betong med slagg innebär detta att en potentiellt betydande hållfasthetstillväxt vid senare åldrar förbises. Denna avhandling undersöker huruvida 56-dygnshållfasthet kan utgöra en lämplig dimensioneringsgrund, och utvärderar de praktiska konsekvenserna avseende hållfasthetsutveckling, armeringsbehov och den inbyggda koldioxidutsläpp.

Laboratoriedata från betongblandningar med GGBS-halter mellan 26% och 51% analyserades och visade en relativ hållfasthetsökning mellan 28 och 56 dygn på ungefär 3–13%. En numerisk modell för hållfasthetsutveckling kalibrerades mot in-situ temperaturmätningar från sex bjälklagsplattor i ett bostadshus uppfört med 32% GGBS-betong. Den kalibrerade modellen tillämpades på tre konstruktionselement, ett filigranbjälklag, en golvplatta och en källarvägg, med vårtemperaturdata från Göteborg som randvillkor.

Resultaten visar att C28/35 med 32% GGBS kan nå den 37 MPa kubhållfasthet som är förknippad med C30/37, men att samtliga undersökta element krävde avsevärt längre tid än 56 dygn under de simulerade förhållandena, med uppskattningsvis 80 dygn som ett mer representativt värde för detta specifika fall. Armeringsbehovet styrdes av böjkapacitet i brottgränstillståndet för bjälklaget, där hållfasthetsklass har liten betydelse, och av sprickbreddskontroll för golvplatta och källarvägg, där skillnaden mellan C28/35 och C30/37 uppgår till 22 mm^2/m.

En minskning av hållfasthetsklass från C30/37 till C28/35 beräknas minska de totala koldioxidekvivalenta utsläppen med ungefär 6% vid nivå 3 och 4% vid nivå 4 klimatprestanda. Studien drar slutsatsen att senare hållfasthetstillväxt i GGBS-betong erbjuder en mätbar potential för effektivare strukturell dimensionering, men att noggrann hänsyn till tidigt beteende, härdningsbetingelser och produktionsförutsättningar krävs innan ett sådant tillvägagångssätt kan tillämpas i praktiken.

Nyckelord: Klimatreducerad betong, GGBS, Tryckhållfasthet, 56-dygnshållfasthet, Dimensionering, Mognadsmetod, Inbyggt koldioxid

Contents

Preface

This master's thesis was carried out at the Department of Architecture and Civil Engineering, Division of Structural Engineering, Chalmers University of Technology, Gothenburg, Sweden. The work was conducted during the spring of 2026.

I would like to express my gratitude to my examiner Carlos Gil Berrocal for his guidance and valuable feedback throughout the work.

Furthermore, I would like to express my sincere appreciation to Nilesh Timmerbäck at Skanska for his patience, support, and valuable insights throughout this work. His experience and guidance have been of great importance for this study.

I would also like to thank Skanska for providing access to laboratory data as well as simulation tools such as PPB and StruSoft, which have been essential for the completion of this thesis.

Gothenburg, June 2026
Saga Sernekvist

Notations

Roman upper case letters

A	Area
A_s	Reinforcement area
$A_{s,min}$	Minimum reinforcement area
A_{ct}	Area of concrete in tension
E	Modulus of elasticity
E_c	Elastic modulus of concrete
E_s	Elastic modulus of reinforcement steel
E_a	Activation energy
$F_{cc,set}$	Compressive strength at setting
GGBS	Ground granulated blast-furnace slag
GWP	Global Warming Potential
GWP-GHG	Greenhouse gas emissions expressed as CO_2-equivalents
K	Earth pressure coefficient
M	Bending moment
M_{Ed}	Design bending moment
N	Normal force
N_{set}	Model parameter for setting behaviour
PPB	Production Planning Concrete
R	Universal gas constant
SLS	Serviceability Limit State
T	Absolute temperature
T_c	Concrete temperature
$T_{c,0}$	Initial concrete temperature
$T_{c,max}$	Maximum concrete temperature
T_{ref}	Reference temperature
ULS	Ultimate Limit State
W_u	Heat of hydration

Roman lower case letters

$a_0(\alpha)$	Hydration rate function
b	Width of section
d	Effective depth
f_c	Compressive strength of concrete
$f_{c,28}$	Compressive strength at 28 days
$f_{c,56}$	Compressive strength at 56 days
f_{ck}	Characteristic compressive strength
f_{cm}	Mean compressive strength
f_{ct}	Tensile strength of concrete
$f_{ct,eff}$	Effective tensile strength of concrete
f_{yd}	Design yield strength of reinforcement
f_{yk}	Characteristic yield strength of reinforcement
h	Height of structural element
p	Pressure

p_{max}	Maximum pressure
p_q	Pressure from surcharge load
p_w	Water pressure
q	Distributed load
s	Model parameter
t	Time
t_1	Time parameter in hydration model
t_e	Equivalent maturity time
$t_{e,ini}$	Initial equivalent maturity time
$t_{e,fin}$	Final equivalent maturity parameter
w	Crack width
w_k	Characteristic crack width
w/c	Water–cement ratio
w/ceq	Equivalent water–cement ratio
z	Lever arm

Greek letters

α	Degree of hydration
β_T	Temperature-dependent maturity factor
β_{RH}	Humidity-dependent maturity factor
β_D	Strength development parameter
γ	Unit weight
γ_w	Unit weight of water
κ	Model parameter
κ_1	Hydration parameter
κ_3	Strength development parameter
σ	Standard deviation
σ_s	Stress in reinforcement
ρ	Reinforcement ratio
ρ_{min}	Minimum reinforcement ratio
Θ	Temperature parameter
Θ_{ref}	Reference temperature parameter

1 Introduction

Concrete is the most widely used construction material worldwide and plays a central role in modern infrastructure and building production. However, the construction sector is also responsible for a significant share of global resource consumption and waste generation. In particular, concrete production contributes substantially to greenhouse gas emissions, primarily due to the manufacturing of Portland cement.

In response to increasing environmental concerns, significant efforts have been made to develop climate-reduced concrete by incorporating Supplementary Cementitious Materials (SCM), such as GGBS. These materials enable a reduction in embodied carbon while maintaining or even improving long-term mechanical performance.

However, the use of such binders introduces new challenges. In particular, climate-reduced concretes often exhibit slower early-age strength development compared to conventional Portland cement concrete. This affects both structural behaviour and construction processes, including formwork removal, load transfer, and production planning. At the same time, the continued strength development beyond 28 days offers potential advantages that are not fully utilised within current design practices.

This master's thesis aims to investigate the challenges and opportunities associated with climate-reduced concrete, with particular focus on strength development and its implications for structural design and construction. The study further evaluates how these material behaviours relate to current design codes and standards, and whether alternative approaches could improve both structural performance and environmental efficiency.

1.1 Background

The compressive strength of concrete is determined according to Eurocode 2 by means of a uniaxial compression test on a standard cylinder specimen with a height of 300 mm and a diameter of 150 mm. The characteristic compressive strength (f_{ck}) at an age of 28 days is defined as the 5th percentile of the strength distribution. This implies that 95% of all tested specimens are expected to exceed this characteristic value, ensuring a statistical safety margin in structural design. Mathematically, the relationship between the mean strength (f_{cm}) and the characteristic strength is expressed as:

$$f_{ck} = f_{cm} - 1.65\sigma \tag{1.1}$$

where σ represents the standard deviation. For standard design classes, Eurocode 2 assumes a fixed difference where $f_{cm} = f_{ck} + 8$ MPa (Al-Emrani et al., 2019).

The choice of 28 days as the reference age is related to the strength development of conventional cement-based concrete during the hydration process. The compressive strength measured after 28 days for ordinary concrete is generally close to the final strength of the material and is therefore used as a representative reference value. However, experimental studies indicate that strength development does not cease at 28 days. For conventional Portland cement concrete, a continued but relatively moderate increase in compressive strength is observed at later ages, with reported gains of approximately 11.5–14.6% between 28 and 365 days (Oner & Akyuz, 2007). At earlier ages, such as 7 days, the achieved strength typically amounts to 20–60% of the final value, depending on the concrete composition and curing conditions. Consequently, the 28-day strength provides a stable and reproducible basis for material classification and structural design of conventional concrete (Konietzky, 2020).

The increasing focus on reducing the environmental impact of concrete has led to a growing interest in the use of supplementary cementitious materials as partial replacements for Portland cement. One of the most commonly used alternative binders is ground granulated blast-furnace slag (GGBS). Slag-based concretes generally exhibit slower early-age strength development compared to conventional Portland cement concrete, while achieving comparable or even higher strength at later ages due to continued hydration and latent hydraulic reactions (Soutsos & Domone, 2018). Since current design practice evaluates concrete strength at 28 days, the additional strength gain occurring beyond this age is often neglected in structural design, despite its potential relevance for material optimisation and environmental performance.

Floor slab systems are of particular interest in this context, as they constitute a large share of a building's total material consumption and embodied environmental impact. The construction sector globally accounts for approximately 40% of total raw material use, and for most floor systems the extraction and production of materials dominate the life-cycle greenhouse gas emissions (Wang et al., 2018). Consequently, even moderate reductions in binder content at the slab level can result in significant reductions in the overall climate footprint of a building.

Foundation elements such as ground slabs and basement walls are also of interest, as they are subjected to moisture and soil pressure, imposing strict requirements on crack width control. The choice of concrete strength class therefore has a direct influence on the reinforcement demand for these elements.

At the same time, longer curing times associated with climate-reduced concretes may introduce practical challenges during construction. The need for shoring posts to remain in place for longer periods can delay construction cycles and increase production costs. This trade-off between reduced environmental impact and increased construction time is therefore an important consideration when evaluating alternative concrete compositions for structural elements.

1.2 Purpose

The increasing use of supplementary cementitious materials, such as ground granulated blast-furnace slag (GGBS), as partial replacements for Portland cement has led to a growing interest in the structural implications of the altered strength development these materials introduce. Since current design practice evaluates concrete strength at 28 days, the additional strength gain occurring beyond this age is typically neglected, despite its potential relevance for material optimisation and environmental performance. The purpose of this study is therefore to evaluate whether 56-day compressive strength can serve as a viable basis for structural design of climate-reduced concrete, and to assess the practical consequences of such an approach with respect to strength development, reinforcement demand, and embodied carbon emissions.

1.3 Goals

The main goal of this study is to investigate the potential of utilising later-age compressive strength in climate-reduced concrete for structural design.

To achieve this, the following specific objectives are defined:

- To analyse the strength development of climate-reduced concrete beyond 28 days based on laboratory data and in-situ measurements.
- To calibrate and evaluate a predictive model for strength development using Produktionsplanering Betong (PPB).
- To assess whether lower concrete strength classes can achieve equivalent performance at 56 days compared to higher classes at 28 days.
- To evaluate the implications of this approach on reinforcement demand in structural design.
- To quantify the potential reduction in CO_2 emissions associated with utilising later-age strength.

1.4 Limitations

The following limitations constraints apply to this study. The PPB simulations are based on a single calibrated material model representing concrete with approximately 32% GGBS replacement. The model is not re-calibrated for mixes with different slag contents, and the results should therefore be interpreted with caution when applied to concretes with significantly higher or lower GGBS levels.

The climate boundary conditions used in the simulations correspond to a spring period in Gothenburg and do not represent winter curing conditions, under which the early-age strength development of slag-containing concretes is known to be more sensitive to temperature. The conclusions drawn regarding the time required to reach a given strength level are therefore not directly transferable to construction activities carried out during colder periods.

The structural analyses are performed on a simplified unit strip model assuming simply supported boundary conditions and uniformly distributed loads. Two-way slab action and partial continuity are not considered.

No cost analysis has been performed. The economic implications of delayed formwork removal, extended curing periods, and potential changes to the construction schedule are discussed qualitatively but not quantified.

2 Theory

This chapter presents the theoretical background relevant to this study. The fundamental mechanisms governing hydration and strength development in concrete are introduced, together with the influence of material composition on the resulting mechanical properties.

Particular attention is given to the use of ground granulated blast furnace slag (GGBS) as a supplementary cementitious material and its influence on early- and long-term strength development. The concepts presented in this chapter provide the foundation for the experimental work and simulations discussed in the subsequent chapters.

2.1 Concrete

The simplest definition of concrete is that it is a mixture of cement, water and aggregates. Although the proportions vary depending on application and strength requirements, the material composition follows relatively consistent ranges. A typical distribution of the main constituents by mass is presented in Table 2.1.

Table 2.1: Typical composition of concrete by mass percentage

Component	Percentage (%)
Cement / Binder	6–16
Water	12–20
Fine aggregate	20–30
Coarse aggregate	40–45

When the water and the cement binds the aggregate particles it forms a monolithic whole. Although only about 6-16 percent of the total concrete mixture is made up by cement, it is still the key component (Soutsos & Domone, 2018).

2.1.1 Cement and Cementitious Materials

The most commonly used type of cement is Portland cement. Its primary reactive constituents are calcium silicates, which are formed during clinker production through high-temperature reactions between calcium oxide and silicon dioxide. These oxides originate from naturally occurring raw materials in the Earth's crust, where calcium oxide is derived from limestone or chalk, and silicon dioxide from clay or shale (Soutsos & Domone, 2018).

The importance of calcium silicates lies in their hydration reactions, which form calcium silicate hydrate (C–S–H). C–S–H constitutes the primary binding phase in hardened cement paste and largely governs both durability-related properties and strength development in concrete. A secondary hydration product is calcium hydroxide (CH), which has limited contribution to mechanical performance and may remain as a comparatively weak phase if it is not subsequently consumed by supplementary reactions (Kurdowski, 2014).

Hydration is inherently time-dependent and is commonly characterised by its rate of heat evolution, reflecting changes in reaction kinetics across distinct stages. These stages occur in parallel with the progressive formation and densification of hydration products, particularly C–S–H and CH (Kurdowski, 2014).

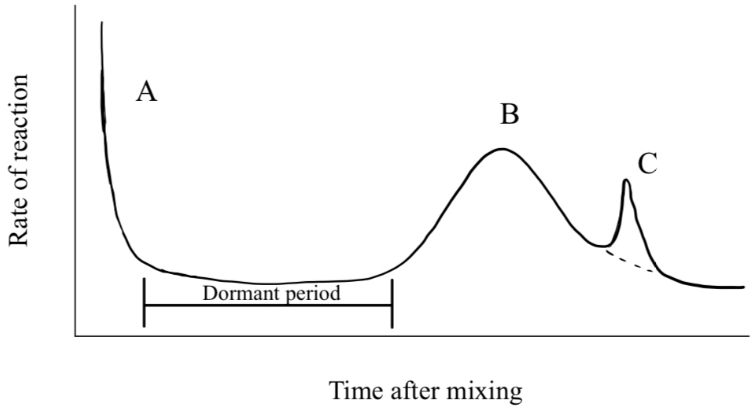

Figure 2.1: Rate of reaction of hydrating cement at constant temperature, illustrating the dormant period and the main reaction stages (A–C). Author's own illustration, inspired by Soutsos & Domone (2018).

Figure 2.1 illustrates the typical stages of cement hydration. The initial peak (A) occurs immediately after mixing and is associated with rapid early reactions, after which the reaction rate decreases and enters a dormant period during which the paste remains workable. This is followed by the main hydration peak (B), which corresponds to the acceleration period and the formation of the load-bearing hydration products, primarily C–S–H, and is closely related to the development of early stiffness and strength. A later, smaller peak (C) may occur after the main peak and is commonly linked to subsequent reactions once sulphate availability is reduced, contributing to continued microstructural development at later ages (Soutsos & Domone, 2018).

Pozzolans

A pozzolan is a material that possesses little or no cementitious value on its own but reacts chemically with calcium hydroxide (CH) in the presence of moisture. Through this pozzolanic reaction, calcium hydroxide is consumed and additional C-S-H is formed, thereby contributing to long-term strength development and improved durability. The most common types of pozzolans are fly ash, ground granulates blast furnace slag (GGBS) and silica fume (Ramezanianpour, 2014).

GGBS is an industrial by-product generated during iron and steel production. It is widely recognised as a sustainable supplementary cementitious material and a partial replacement for traditional Portland cement (Zhou et al., 2026).

In order for blast-furnace slag to exhibit cementitious properties, it must be finely ground to a high specific surface area, typically in the range of 600–650 m^2/kg. This is significantly higher than for Portland cement, which commonly has a specific surface area of approximately 260–280 m^2/kg (Jeremi et al., 2026). It is through this fine grinding process that the slag becomes reactive and capable of participating in pozzolanic and latent hydraulic reactions.

Although the grinding process requires additional energy input, the overall energy demand for producing GGBS is substantially lower than for Portland cement. Previous studies have shown that the total energy consumption associated with GGBS production is approximately 31.5% lower compared to conventional Portland cement (Jeremi et al., 2026).

2.1.2 Strength Development of Concrete

The hardening process for portland cement occurs right as the silicates react with water, immediately forming C-S-H. GGBS on the other hand hardens after the silicates in the cement have produced calcium hydroxide which the GGBS then reacts with, resulting in slower rate of hardening when incorporated (Ramezanianpour, 2014).

Effect of ambient temperature

When the ambient temperature is increased (with +20 °C treated as a neutral reference), early-age hydration reactions are accelerated. This is reflected by a higher heat flow rate and a shortened dormant period, indicating that the main hydration peak occurs earlier and that early strength development is reached sooner (Hafiz et al., 2020).

Conversely, at lower ambient temperatures the heat release is delayed and the early-age reaction rate is reduced, which postpones the development of stiffness and compressive strength during the first days after casting (Hafiz et al., 2020). In a study by Hafiz et al., this effect is clearly observed as a systematic shift of the first hydration peak towards later ages when the initial ambient temperature is reduced, demonstrating the strong sensitivity of early-age hydration kinetics to temperature.

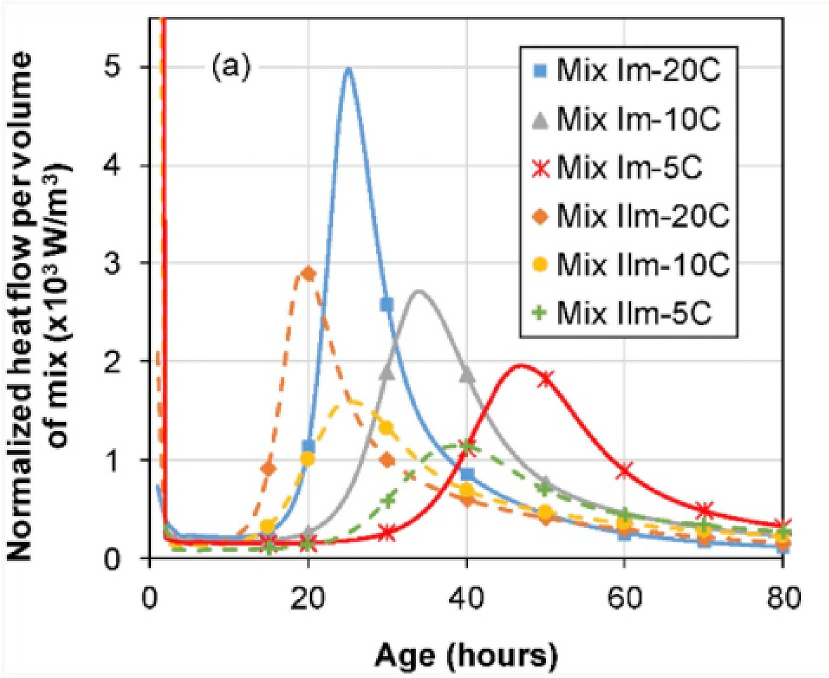

Figure 2.2: Example of isothermal calorimetry tests illustrating delayed early-age hydration at lower curing temperatures, shown through heat flow curves as a function of time. Reproduced from Hafiz et al. (2020) (Fig. 2a) under the terms of the Creative Commons CC BY-NC-ND license.

28-day compression strength

Regular concrete using Portland cement gains strength very quickly. The compressive strength of concrete is determined using standardized tests using a cylinder with the measurements 150 mm diameter and 300 mm in height. When talking about the strength of the concrete the period 28-days is often mentioned, which comes from the fact that tests have shown that 95 percent of concrete exceed the compressive strength given as the characteristic compressive strength after 28 days (Al-Emrani et al., 2019).

Based on the 28-day compressive strength, concrete is classified into standardized strength classes, which form the basis for structural design and material specification. Each concrete class is defined by its characteristic compressive strength, expressed as the 5% fractile of test results obtained at 28 days. This means that 95% of all specimens are expected to achieve a compressive strength equal to or greater than the specified characteristic value.

The strength class designation follows the notation C*x*/*y*, where *x* represents the characteristic compressive strength measured on a standard cylinder (150 mm diameter, 300 mm height), and *y* corresponds to the characteristic strength measured on a standard cube (150 mm). These strength classes are used consistently in structural design codes to determine material properties such as elastic modulus and tensile strength, thereby providing a unified and reliable basis for comparing different concrete mixes and ensuring adequate structural performance.

Table 2.2: Common concrete strength classes and corresponding characteristic compressive strengths at 28 days.

Concrete class	Cylinder strength f_{ck} [MPa]	Cube strength $f_{ck,cube}$ [MPa]
C25/30	25	30
C28/35	28	35
C30/37	30	37
C35/45	35	45
C32/40	32	40
C40/50	40	50
C45/55	45	55
C50/60	50	60
C55/67	55	67

Compressive strength of GGBS concrete

As discussed in Chapter 2.1.2, concrete incorporating GGBS exhibits a distinct time-dependent compressive strength development compared to conventional Portland cement concrete. At early ages (approximately 7–28 days), GGBS concretes generally display lower compressive strength, while at later ages the strength development accelerates and may surpass that of corresponding reference mixes. The long-term strength gain is particularly pronounced for mixtures with higher GGBS contents, which show a larger relative increase in strength between early and mature ages (Oner & Akyuz, 2007).

Previous studies further indicate that there exists an optimum GGBS replacement level with respect to compressive strength. The highest long-term strength is typically obtained when GGBS constitutes approximately 55–59% of the total binder content. At this replacement level, the contribution of GGBS to the load-bearing cementitious matrix is maximised. When the GGBS content exceeds this range, the compressive strength tends to decrease, as the excess slag no longer contributes effectively to strength development and instead behaves primarily as an inert filler. Consequently, very high GGBS replacement levels may be disadvantageous from a mechanical performance perspective, despite their environmental benefits (Oner & Akyuz, 2007).

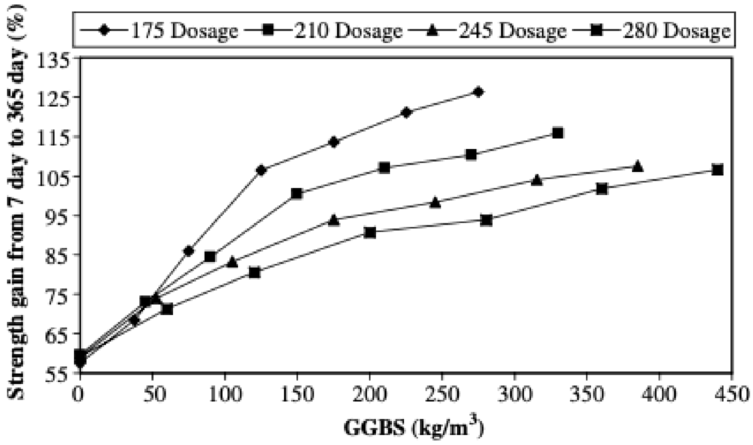

Figure 2.3: Relative compressive strength gain between 7 and 365 days for concretes with varying GGBS contents and total binder dosages. The figure illustrates the pronounced long-term strength development of GGBS concretes compared to early-age performance. Adapted from Oner and Akyuz (2007).

This behaviour is illustrated in Figure 2.3, where several concretes with high GGBS replacement levels exhibit a relative compressive strength exceeding 100% at one year when compared with their 7-day strength.

2.1.3 Exposure- and Curing Classes

Exposure classes are a standardised classification system used to describe the environmental conditions to which a concrete structure is subjected (Svenska Betongföreningen, 2009). Each class is denoted by a two-letter prefix indicating the governing degradation mechanism, as summarised in Table 2.3.

Table 2.3: Exposure class prefixes and corresponding degradation mechanisms

Prefix	Degradation mechanism
XC	Carbonation-induced corrosion
XD	Corrosion induced by chlorides from de-icing agents
XS	Corrosion induced by chlorides from seawater
XF	Freeze-thaw attack
XA	Chemical attack

The numerical suffix following the prefix indicates the severity of the exposure, with higher numbers denoting more aggressive conditions (Svenska Betongföreningen, 2009). For carbonation-induced corrosion, the most severe condition corresponds to a cyclically wet and dry environment, classified as XC4. For chemical attack, the highest severity class, XA3, denotes a strongly aggressive chemical environment.

Current Swedish standards impose restrictions on the proportion of supplementary cementitious materials (SCMs) that may constitute the total binder content, with limits linked to the applicable exposure class. For GGBS, the permitted proportion ranges from 65 to 70% of the total binder content, depending on exposure class (SIS – Swedish Institute for Standards, 2025).

Curing classes define the minimum duration for which freshly cast concrete must be protected against premature drying, frost, and other adverse environmental conditions (SIS – Swedish Institute for Standards, 2009). The classification system consists of four classes, as presented in Table 2.4, where Class 1 specifies a minimum curing period expressed in hours, while Classes 2 through 4 instead define the required curing duration in terms of a minimum percentage of the specified characteristic compressive strength at 28 days.

Table 2.4: Curing classes according to SS-EN 13670

	Curing class 1	**Curing class 2**	**Curing class 3**	**Curing class 4**
Period (hours)	12[a]	Not applicable	Not applicable	Not applicable
Strength at 28 days (% of f_{ck})	Not applicable	35%	50%	70%

[a] Provided that the setting time does not exceed 5 hours and the concrete temperature is equal to or greater than 5°C.

According to AMA Anläggning 23, curing class 1 is generally considered sufficient for concrete in exposure classes X0 and XC1. For exposure class XC2, a minimum of curing class 2 is recommended, while all other exposure classes require at least curing class 3 (Svensk Byggtjänst, 2023).

Several methods suitable for curing concrete in practice are identified in Annex F of SS-EN 13670, including retaining the formwork in place, covering the concrete surface with vapour-tight sheeting secured at edges and joints to prevent draughts, applying moist covering materials protected against drying, maintaining a visibly wet surface through continuous water spraying, and applying a curing membrane of proven suitability (SIS – Swedish Institute for Standards, 2009). These methods may be employed individually or in sequence, depending on the conditions at the time of casting.

2.1.4 Climate levels

When selecting the amount of supplementary cementitious materials in a concrete mix, the choice is often governed by the desired level of climate improvement defined by the Swedish Concrete Association. In the guidance document *Vägledning Klimatförbättrad betong* (Svensk Betong, 2025), climate-improved concrete is classified into four levels, where each level represents a progressively lower climate impact compared to a reference value representing commonly used concrete mixes in Sweden.

The climate impact is expressed as GWP-GHG (kg CO_2-eq/m^3) and includes emissions from the product stage modules A1–A3. These modules cover raw material supply (A1), transport of raw materials to the concrete plant (A2), and manufacturing of the concrete (A3). Together, these stages represent the embodied carbon of the concrete up to the factory gate and form the basis for comparison between different concrete mixes.

Table 2.5: Climate impact GWP-GHG (kg CO_2-eq/m^3) according to Svensk Betong, Ready-Mixed Concrete Table 1.

	Exposure class	Strength class	w/c$_{eq}$*	Industry reference	Level 1	Level 2	Level 3	Level 4
1. Indoor concrete								
RH$_{req}$ < 85%								
	X0, XC1	C50/60	0.32	345 (385)	310 (345)	280 (310)	245 (270)	$\leq$ 210 (230)
			0.35	330 (365)	295 (330)	265 (290)	230 (255)	$\leq$ 195 (220)
			0.40	310 (340)	280 (305)	250 (270)	215 (240)	$\leq$ 185 (205)
RH$_{req}$ < 90%								
	X0, XC1	C35/45	0.45	275 (305)	250 (275)	220 (245)	195 (215)	$\leq$ 165 (185)
			0.50	255 (280)	230 (255)	205 (225)	180 (195)	$\leq$ 150 (170)
2. Indoor concrete								
Low humidity								
	X0, XC1	C30/37	0.55	230 (255)	205 (230)	185 (205)	160 (180)	$\leq$ 135 (155)
	X0, XC1	C28/35	0.60	215 (240)	195 (215)	175 (190)	150 (170)	$\leq$ 130 (145)
	X0, XC1	C25/30	0.65	205 (225)	185 (205)	165 (180)	145 (160)	$\leq$ 125 (135)
	X0, XC1	C16/20	0.70	185 (205)	165 (185)	150 (165)	130 (145)	$\leq$ 110 (125)
3. Foundation structures								
Frost-free								
	XC1	C30/37	0.55	230 (255)	205 (230)	185 (205)	160 (180)	$\leq$ 135 (155)
Non frost-free								
	XC3, XC4, XF3	C28/35	0.55**	245 (270)	220 (245)	195 (215)	170 (190)	$\leq$ 145 (160)
4. Outdoor concrete								
External walls, balconies								
	XC3, XC4, XF3	C28/35	0.55**	245 (270)	220 (245)	195 (215)	170 (190)	$\leq$ 145 (160)

* Typical values/classes. Primarily governed by exposure class and strength requirements. ** Maximum w/c$_{eq}$ in the exposure class according to SS 137003:2021 and the Swedish Transport Administration. Net value is reported with gross value in parentheses.

The levels are defined relative to an industry reference, which represents typical concrete compositions used in Sweden prior to the widespread implementation of climate-reduced solutions. As shown in Table 2.5, each successive level corresponds to a reduction in climate impact compared to this reference, which is primarily achieved through increased use of supplementary cementitious materials such as GGBS. Consequently, concretes within the same strength class may exhibit significantly different climate impacts depending on the selected level.

2.1.5 Cracks

Cracking in concrete occurs when tensile stresses reach the tensile strength of the material. These stresses may be caused by external actions (bending, direct tension, shear) or by restraint effects, where shrinkage or temperature-induced deformations are prevented. Typical crack types include flexural cracks, flexural–shear cracks, and web shear cracks, depending on where cracking initiates and how the stress field develops (Al-Emrani et al., 2019).

Cracking changes structural behaviour by reducing stiffness and increasing deflections, since reinforcement must carry most tensile forces after cracking and load transfer becomes more truss-like through diagonal concrete compression struts. Cracks also influence durability by providing paths for ingress of detrimental substances and increasing the risk of reinforcement corrosion, although very fine cracks may partially seal over time. Reinforcement primarily serves to control cracking by promoting many fine cracks rather than a few wide ones (Al-Emrani et al., 2019).

The transition from an uncracked to a cracked structural state is commonly described in terms of three behavioural stages in reinforced concrete. In *Stage I* (uncracked state), concrete and reinforcement act compositely and the stress–strain distribution remains essentially linear, with the tensile zone still carried by the concrete. In *Stage II* (cracked state), flexural cracks form once the tensile stress exceeds the cracking resistance, and the tensile force is primarily transferred to the reinforcement while the concrete in tension is typically neglected in sectional analysis. In *Stage III* (ultimate stage), increasing loading leads to nonlinear material behaviour and yielding of the reinforcement and/or nonlinear compression response in concrete, governing the approach to ultimate capacity and failure (Al-Emrani et al., 2019).

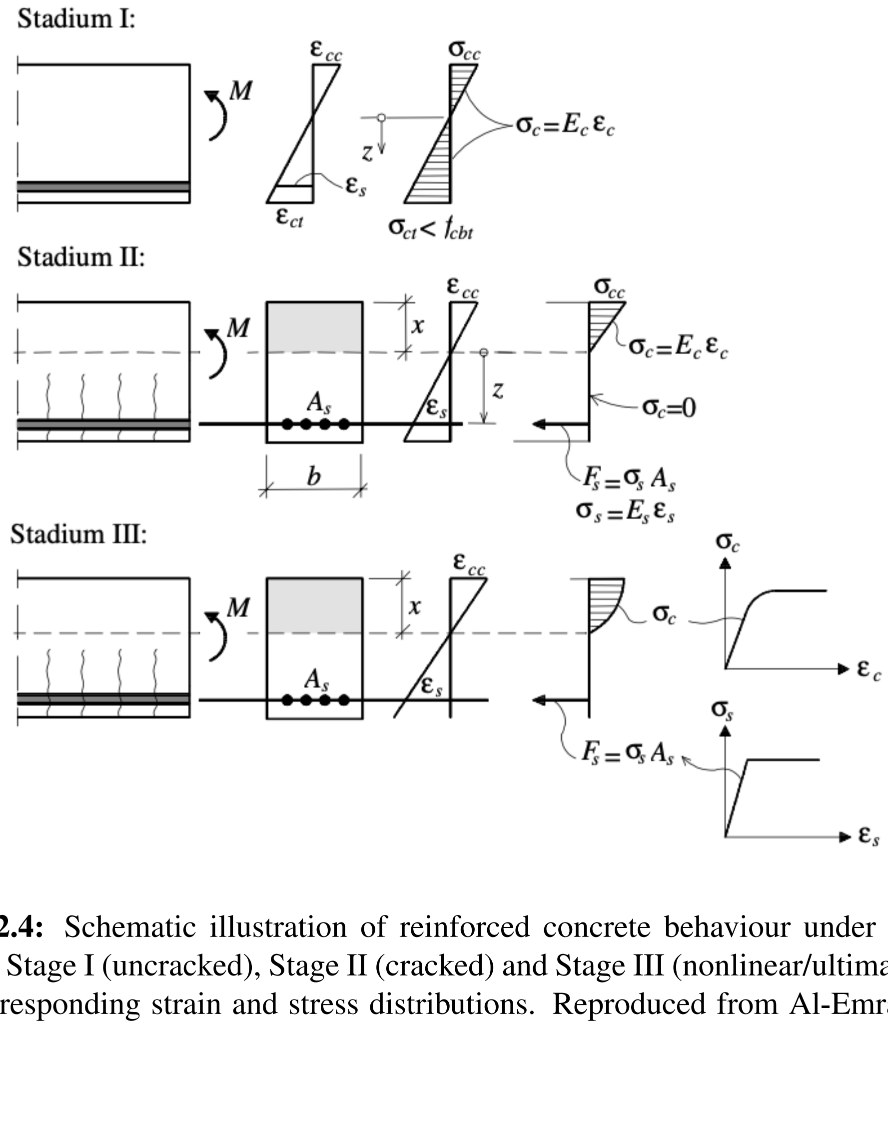

Figure 2.4: Schematic illustration of reinforced concrete behaviour under bending, showing Stage I (uncracked), Stage II (cracked) and Stage III (nonlinear/ultimate stage) with corresponding strain and stress distributions. Reproduced from Al-Emrani et al. (2019).

Early age cracking

During the hydration phase of the hardening process, concrete releases most of its heat. When the concrete subsequently cools, the tendency for contraction is significant. In cases where the concrete is restrained, for example in basement walls, high tensile stresses may develop. This phenomenon becomes more pronounced as the number of restrained surfaces increases (Engström, 2014).

Since the governing factors for this phenomenon are internal heat generation in combination with early formwork removal, it may appear counterintuitive that concretes with high incorporations of GGBS have been shown to be more susceptible to restraint cracking (Sundelius & Wahlqvist, 2022). This can be explained by the relationship between tensile stress and strength development. Although the heat generated during hydration is significantly lower when using GGBS, the early-age strength development is also slower.

Different exposure classes impose different requirements regarding acceptable stress-to-strength ratios. In the study performed by Sundelius and Wahlqvist (2022), where different basement wall thickenesses were analysed, and the influence of slagg was analyzed, the results showed that a concrete with 50% GGBS exhibited a higher stress-to-strength ratio than Portland cement concrete when examined at 20 °C. For the colder case, at -1 °C, the stress-to-strength ratio was generally lower for most wall thicknesses, however, for thinner wall structures (250–500 mm), the hydration process was so slow that the structure did not reach a minimum compressive strength of 5 MPa before the temperature dropped below 0 °C.

2.2 The Construction Process

The construction process of a building project can generally be divided into a number of main stages, ranging from early project development and design to on-site production and completion. Each stage contributes differently to the total project cost and has varying potential to influence both economic and environmental performance.

Studies of residential construction projects in Sweden show that the total production cost is typically dominated by the construction phase itself, which accounts for approximately 55–60% of the total cost. Developer-related costs, including land acquisition, administration and design, represent around 20–25%, while value-added tax constitutes roughly 15–20% of the total production cost (Johnsson, 2017). Although the design and planning stages represent a relatively small share of the total cost, decisions made during these early phases strongly influence costs incurred later in the project.

The construction phase is particularly sensitive to time-related disturbances. Delays during on-site production can lead to increased costs through extended site establishment, higher labour and equipment costs, and increased financing costs. In addition, prolonged construction time may result in higher environmental impact, as emissions from machinery, transport and temporary works accumulate over time. Previous research has shown that efforts to accelerate construction activities often involve trade-offs between time, cost and CO_2 emissions, where reducing construction time may increase both direct costs and emissions if more resource-intensive methods are adopted (Surapha & Sutheerawatthana, 2024).

2.2.1 Temporary structures

During the construction phase, a shoring post is a temporary, height-adjustable telescopic steel support used to provide stability during critical stages. Its primary function is to carry the loads from newly cast concrete, associated formwork, and supporting joists until the concrete has gained sufficient strength to become self-supporting (Buitrago et al., 2020).

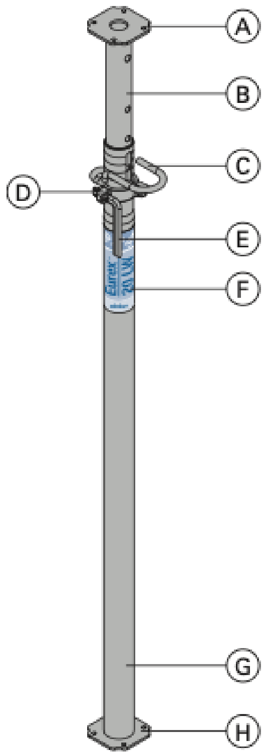

Figure 2.5: Main components of a construction prop (Doka Eurex 20 LW), showing the labelled parts A–H referenced in this thesis. Adapted from Doka GmbH (2024), p. 7.

A typical shoring post used for temporary shoring during concrete works typically consists of the following main components:

- A — Top plate: Upper bearing surface providing contact to the supported element.
- B — Inner tube: Telescopic inner member used for coarse height adjustment.
- C — Retaining clamp / fixing pin: Locking pin securing the inner tube at the selected coarse height.
- D — Adjusting nut: Threaded nut used for fine height adjustment once the prop is positioned.
- E — Handle / knob: Integrated handle used to rotate the adjusting nut during installation and adjustment.
- F — Type sticker: Identification label indicating the prop type and relevant technical specifications.
- G — Outer tube: Main load-carrying outer tube providing overall stiffness and guiding the inner tube.
- H — Base plate: Lower bearing surface transferring load to the supporting ground.

The required amount and arrangement of shoring posts depends on the structural layout and loading conditions. In particular, the symmetry and geometry of the building element influence how loads are distributed and transferred during the temporary construction phase. The number of props is therefore governed by the magnitude of the construction loads acting on each support, together with the load-bearing capacity of the selected shoring posts and their allowable spacing (Ljungkrantz et al., 1992).

2.2.2 Temporary construction process

Once the shoring posts have been installed, they are intended to remain in place during the early-age phase when the concrete is still gaining stiffness and load-bearing capacity. Unless otherwise specified in the execution specification or by the structural designer, the temporary supports should not be removed until the concrete has achieved a sufficient compressive strength to safely carry the relevant construction loads. A commonly applied criterion is that the concrete should reach at least 70% of the required final compressive strength before de-shoring is carried out, as this indicates that the structural element has developed adequate capacity to support its self-weight and associated loads during the subsequent construction stages (SIS – Swedish Standards Institute, 2015).

In a study conducted by Olsson, 2019, the effects of early de-shoring were analysed using numerical modelling of multi-storey concrete buildings. The results showed that even when de-shoring was performed at a concrete strength level of approximately 50% of the 28-day compressive strength, the resulting initial deflections were relatively small and generally not governing. Instead, the critical consequence of early de-shoring was identified as an increased risk of cracking above load-bearing walls, where restraint effects lead to elevated tensile stresses in the slab.

The study further investigated different shoring strategies, including the use of safety shoring (reshoring) and variations in the number of supported floors. In multi-storey concrete construction, it is common practice to maintain shoring or safety shoring over several lower floors in order to distribute the loads from newly cast slabs in a controlled manner. According to practical guidelines from formwork suppliers, such as Doka, shoring is typically maintained over four to five storeys to ensure that construction loads are effectively transferred through the structure without overloading individual slabs (Doka GmbH, 2020).

To compensate for the slower early-age strength development of GGBS concrete, an increased number of shored floors could potentially be considered as a compensating measure. Any increase in shoring would likely have implications for construction-phase costs and efficiency, which are assessed later in this study.

2.2.3 Temporary wall structures

Among the most common wall types in multi-storey residential buildings are non-load-bearing infill walls (utfackningsväggar). These walls are designed to carry only their self-weight and wind loads, while all vertical loads are transferred through the building's primary load-bearing structural system, typically consisting of an internal core or frame (Pettersson & Strömberg, 2013).

Other commonly used wall systems include sandwich walls, which are prefabricated concrete elements consisting of two concrete layers with an intermediate layer of thermal insulation (Lättklinkerbetong AB, 2020), and double-skin walls (skalväggar). The latter are composed of two thin prefabricated concrete shells that are assembled on site and subsequently filled with cast-in-place concrete, resulting in a monolithic wall with increased stiffness and structural capacity (Skandinaviska Byggelement AB, 2016).

Regardless of the type of wall element used, temporary supporting structures are required during construction. Their primary function is to maintain the walls in an upright and stable position during the construction phase, when the walls are exposed to wind loads and concrete pressure prior to the completion of the permanent structural system.

These temporary support systems vary depending on wall type, but typically consist of adjustable assembly supports, commonly referred to as wall braces or mounting supports. Such supports are technical auxiliary structures designed to temporarily brace and align prefabricated concrete or steel walls during erection, allowing both coarse and fine adjustment of the wall position (Formmax AB, 2014).

Figure 2.6: Main components of a temporary wall support (slanted prop), showing the principal elements used for stabilisation and alignment of prefabricated wall elements during erection. Adapted from Schake GmbH (2024).

The assembly supports are anchored between the wall element and the floor slab below, which implies that the underlying slab must have attained sufficient early-age compressive strength to safely resist the forces introduced by the supports. This requirement is critical for maintaining the planned construction takt, as wall erection cannot commence until the slab has reached the required strength level.

In practice, this is commonly verified through on-site pull-out testing of anchors installed in the slab, ensuring that the concrete can safely transfer the forces associated with temporary wall supports (Hilti Group, 2024).

Consequently, the rate of strength development of the concrete plays a decisive role in the construction sequence. In particular, the use of ground granulated blast-furnace slag (GGBS) as a cement replacement may delay early-age strength gain, which can postpone wall erection. Any delay in erecting walls subsequently delays the casting of the next floor slab, leading to a shift in the entire production schedule.

2.2.4 Takt Planning and Its Relation to Concrete Hardening

Takt planning is a production planning and control method that aims to create a predictable and repetitive rhythm in the construction process by dividing the project into predefined zones and assigning a fixed time interval, referred to as takt time, to each zone (Bokelid & Fayed, 2022). The method has its origins in industrial manufacturing but has been adapted to construction, where trades move between fixed locations rather than products moving along an assembly line.

In building projects involving cast-in-place concrete, takt planning is closely linked to the time-dependent development of material properties. Several construction activities, such as removal of formwork, de-shoring, and erection of subsequent structural elements, are governed not only by calendar time but also by the concrete's achieved strength level. Consequently, the assumption of a fixed takt time implicitly relies on an expected rate of hardening and strength development (Bokelid & Fayed, 2022).

In conventional construction practice, takt times are often calibrated based on experience with Portland cement concrete under moderate curing conditions. However, when alternative binder compositions are used, such as concrete with high levels of ground granulated blast-furnace slag (GGBS), or when curing takes place at low ambient temperatures, the early-age strength development may be significantly delayed. This can result in situations where the planned takt time no longer aligns with the actual state of the structure, as the concrete may not have reached the required strength to safely proceed with the next construction stage.

From a takt planning perspective, this introduces a potential mismatch between the planned production rhythm and the physical constraints imposed by material behaviour. If the takt is maintained despite insufficient concrete strength, there is a risk of premature loading, increased cracking, or unsafe removal of temporary supports. Conversely, if the work must be paused to await sufficient hardening, the takt-train is interrupted, leading to delays that may propagate through subsequent zones and trades (Bokelid & Fayed, 2022).

2.3 Produktionsplanering Betong (PPB)

Produktionsplanering Betong (PPB) is an open-source software developed by the Development Fund of the Swedish Construction Industry (SBUF). The software can be used for several analyses related to concrete structures, including temperature development, maturity calculations and strength prediction (Svenska Byggbranschens Utvecklingsfond, n.d.).

In this thesis, PPB has primarily been used to predict the long-term strength development of concrete and to evaluate how well the numerical model reproduces experimentally obtained results.

2.3.1 Maturity and Strength Model in PPB

The modelling approach implemented in PPB follows the principles presented in *Concrete Handbook – Materials*, Chapter 16 (Ljungkrantz et al., 1994).

When cement comes into contact with water, hydration reactions are initiated and hydration products, primarily C–S–H gel, are formed. The reactions are exothermic and release heat, commonly referred to as the heat of hydration. The total released heat is, in first approximation, proportional to the cement content. In temperature analyses of early-age concrete, the heat of hydration is therefore treated as internally generated heat. The rate of heat generation is proportional to the rate of hydration and thereby to the rate of change of the degree of hydration. The degree of hydration, α, represents the fraction of cement that has reacted at a given time. The hydration rate can be expressed as

$$\frac{d\alpha}{dt} = a_0(\alpha)\, \beta_T\, \beta_{RH} \tag{2.1}$$

where $a_0(\alpha)$ is a material-specific hydration rate function depending only on the cement composition and the current degree of hydration, β_T is a temperature-dependent rate factor, and β_{RH} is a humidity-dependent rate factor. The function $a_0(\alpha)$ describes the hydration rate under reference conditions and depends only on α.

The temperature factor β_T is commonly expressed using an Arrhenius-type relationship

$$\beta_T = \exp\left[\frac{E_a}{R}\left(\frac{1}{T_{ref}} - \frac{1}{T}\right)\right] \tag{2.2}$$

where E_a is the apparent activation energy, R is the universal gas constant, T is the absolute temperature and T_{ref} is the reference temperature. By separating variables, the expression may be written as

$$\frac{d\alpha}{a_0(\alpha)} = \beta_T\, \beta_{RH}\, dt \tag{2.3}$$

Integration from the initial state to time t gives

$$\int_0^{\alpha} \frac{d\alpha}{a_0(\alpha)} = \int_0^{t} \beta_T\, \beta_{RH}\, dt \tag{2.4}$$

The left-hand side is a monotonically increasing function of the degree of hydration, since $a_0(\alpha) > 0$ during hydration. The right-hand side consists of the integral of the temperature- and humidity-dependent rate factors and has the dimension of time. Since this integral has the physical unit of time, it is natural to introduce the concept of maturity time, defined as

$$t_e = \int_0^{t} \beta_T\, \beta_{RH}\, dt + \Delta t_e(0) \tag{2.5}$$

where $\Delta t_e(0)$ represents any initial maturity at the reference time.

The equivalent maturity time may thus be interpreted as the storage time the concrete would have required under reference conditions (typically +20°C and sufficient moisture) to reach the same degree of hydration as under the actual temperature and humidity history. Strength development can therefore be expressed as a function of equivalent maturity time rather than real time,

$$f_c = f_c(t_e) \tag{2.6}$$

which enables the influence of varying temperature conditions to be incorporated into a single time parameter.

3 Methodology

This study is structured around four main components: calibration of a numerical strength development model, simulation of structural elements in a case study building, and assessment of reinforcement demand and embodied carbon emissions.

Laboratory Data and Strength Development Beyond 28 Days

Compressive strength data from cube specimens were collected for a range of climate-reduced concrete mixes, covering varying strength classes, water-to-binder ratios, and GGBS replacement levels. The data were used to investigate the continued strength development beyond 28 days and to provide a basis for evaluating the predictive capability of the numerical model.

Calibration of Numerical Model

Strength development data recorded during the casting of a multi-storey residential building were used to calibrate the numerical model. The building was constructed using concrete with approximately 32% GGBS replacement, and temperature sensors were installed in several floor slabs during curing. The recorded temperature histories were converted into maturity-based strength development using the Arrhenius formulation applied in the ConReg 806 measurement system.

The starting point for the calibration was a mix recipe in PPB corresponding to a Level 4 climate-improved concrete. Model parameters were subsequently adjusted based on the sensitivity analysis presented in an existing Monte Carlo study, until satisfactory agreement was obtained between the simulated and measured strength development curves. The calibrated model was then evaluated against the laboratory cube data by modelling a $150 \times 150 \times 150$ mm cube in PPB under controlled conditions of +20°C. Only the basic mix parameters, water-to-binder ratio, strength class, and 28-day compressive strength, were varied between mixes, while the calibrated material parameters were kept unchanged. This allowed an assessment of how well a model calibrated for 32% GGBS can estimate later-age strength gain for mixes with different binder compositions.

Case Study — Strength Development in Structural Elements

The calibrated model was applied to three structural elements from an existing residential building: a filigree floor slab, a ground slab, and a basement external wall. Each element was modelled in PPB according to its geometry and assumed casting conditions, using measured temperature data from a weather station in Gothenburg covering the period April–June as representative spring curing conditions.

For each element, three concrete scenarios were compared: conventional Portland cement concrete (C30/37), the calibrated 32% GGBS model (C30/37), and the same GGBS model at a reduced strength class (C28/35). The primary objective was to assess whether the lower strength class concrete, when evaluated at 56 days rather than 28 days, can achieve a compressive strength equivalent to the 28-day strength of the higher class, specifically, whether C28/35 with 32% GGBS can reach 37 MPa at 56 days.

Reinforcement Demand

The influence of concrete strength class on reinforcement demand was investigated for the structural elements. The required reinforcement was assessed with respect to four criteria: minimum reinforcement for crack width control, crack width verification in SLS, ULS bending resistance, and SLS deflection. By comparing the reinforcement demand for C28/35 and C30/37, the study identifies cases where the choice of strength class has a meaningful influence on the required reinforcement and cases where the effect is negligible.

Environmental Impact

The potential reduction in embodied carbon emissions associated with specifying a lower concrete strength class was quantified based on published emission values for factory-mixed concrete from Svensk Betong. The analysis covers the three structural elements included in the case study and considers both the reduction in concrete emissions and the marginal change in reinforcement demand resulting from the changed strength class.

4 Laboratory Strength Development Beyond 28 Days

The characteristic compressive strength of concrete is conventionally defined at 28 days. As a consequence, standard laboratory testing is typically terminated at this age, and the continued strength development at later ages is seldom systematically evaluated.

In the present study, selected concrete mixes were tested beyond 28 days in order to investigate the later-age strength development, with particular focus on concretes containing GGBS. The curing period was extended up to 56 days for most mixes, and up to 90 days for one mix. The investigated mixes had GGBS replacement levels ranging from 26% to 51%, water-to-binder ratios between 0.40 and 0.55, and belonged to strength classes between C30/37 and C45/55.

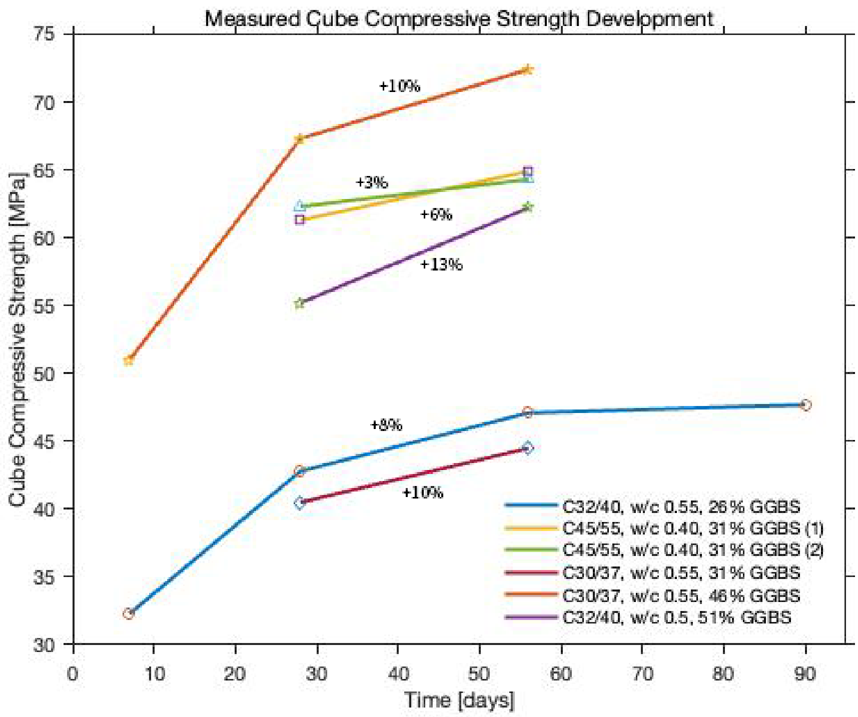

Figure 4.1: Measured compressive strength and relative strength increase between 28 and 56 days calculated from laboratory measurements.

Figure 4.1 illustrates the measured cube compressive strengths and their development beyond 28 days. It can be observed that all investigated mixes exceed their nominal strength class already at 28 days. No clear correlation is identified between the specified strength class and the measured compressive strength for the tested mixes. This is consistent with the definition of strength classes, where the characteristic strength represents a lower fractile value, meaning that the majority of test results are expected to exceed the specified class strength.

Table 4.1: Overview of investigated concrete mixes and observed strength development beyond 28 days.

Parameter	Minimum	Maximum
GGBS content [%]	26	51
Strength class	C30/37	C45/55
Water–cement ratio, w/c [-]	0.40	0.55
28-day cube strength [MPa]	40.5	67.3
56-day cube strength [MPa]	44.5	72.4
Absolute strength increase (28–56 d) [MPa]	2.0	7.0
Relative strength increase (28–56 d) [%]	3.21	12.68

Table 4.1 summarises the range of investigated mixes and the observed strength development beyond 28 days. The results show a significant variation in both absolute and relative strength increase between mixes. In particular, the relative strength gain between 28 and 56 days ranges from approximately 3% to 12%, highlighting that the magnitude of later-age strength development is highly dependent on the specific mix composition.

5 Measured Data and Model Calibration

This chapter presents a case study of a residential building constructed using concrete with 32% GGBS replacement. The internal temperature development of six structural slabs was continuously monitored during curing. The recorded temperature histories were subsequently converted into equivalent maturity-based strength development in order to evaluate the in-situ strength evolution.

The investigated slabs are denoted BJL3–BJL8 and were cast using the same concrete mix. A summary of the relevant input parameters is provided in Table 5.1.

Table 5.1: Input parameters for the investigated slabs in the case study.

Parameter	Value
Concrete strength class	C30/37
Water–cement ratio, w/c [-]	0.55
GGBS replacement level [%]	32
Slab thickness [mm]	400
Number of slabs	6
Slab identification	BJL3–BJL8

5.1 Maturity Function Used in the Measurements

During curing of the slab, three temperature sensors were installed, positioned as illustrated in Figure 5.1. The top and bottom sensors were placed approximately 5 cm from the respective concrete surfaces, while the middle sensor was located near the mid-depth of the slab.

The recorded temperature histories were subsequently converted into equivalent maturity time using the ConReg 806 system. ConReg 806 complies with ASTM C1074, which is the standard practice for estimating concrete strength based on the maturity method.

ASTM C1074 permits both the Nurse–Saul temperature-time factor method and the Arrhenius equivalent age formulation (ASTM C1074-19e1, 2019). Following communication with representatives from the supplier (personal communication, 2026), it was clarified that the ConReg 806 system applies an Arrhenius-based maturity formulation. The temperature dependency of the maturity function is therefore described by the Arrhenius relationship presented in Equation 2.2.

Furthermore, according to the supplier (personal communication, 2026), the ConReg 806 system can be regarded as a predecessor to the PPB framework and was developed in collaboration with researchers who later contributed to the development of PPB.

This implies that both ConReg 806 and PPB rely on the same fundamental Arrhenius-based maturity equation. Although minor differences in implementation, calibration procedures, or parameter selection may exist between the two systems, such variations are considered negligible within the scope of this study.

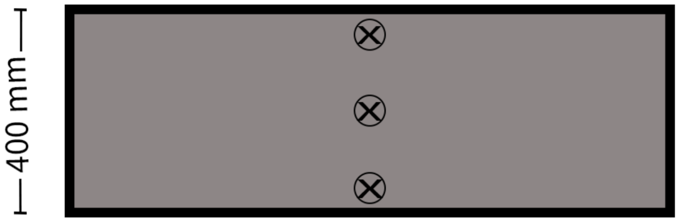

Figure 5.1: Position of the temperature sensors in the cross-section of the concrete specimen.

5.2 Temperatures During The Curing

During the curing of the investigated slabs, temperature measurements were continuously recorded. In order to describe the thermal boundary conditions influencing strength development, the measured data were processed into representative temperature parameters.

For each slab, the following values were given:

- The initial concrete temperature, $T_{c,0}$,
- The maximum concrete temperature reached during curing, $T_{c,\max}$,
- The average ambient air temperature for the intervals 1–7, 8–14, 15–21 and 21–28 days.

These parameters were used as input data in the numerical simulations performed in PPB. The compiled temperature data are presented in Table 5.2.

Table 5.2: Temperature data for investigated slabs (BJL)

BJL	$T_{c,0}$ (°C)	$T_{c,\max}$ (°C)	T_o day 1–7 (°C)	T_o day 8–14 (°C)	T_o day 15–21 (°C)	T_o day 21–28 (°C)
BJL 3	16.6 °C	30.0 °C	9.4 °C	6.2 °C	–	–
BJL 4	13.3 °C	17.0 °C	2.74 °C	5.18 °C	1.69 °C	0.61 °C
BJL 5	17.0 °C	26.8 °C	1.58 °C	6.03 °C	5.89 °C	4.65 °C
BJL 6	13.0 °C	24.2 °C	6.05 °C	4.65 °C	1.11 °C	1.11 °C
BJL 7	13.4 °C	19.0 °C	4.46 °C	1.86 °C	-0.015 °C	-3.37 °C
BJL 8	20.0 °C	31.5 °C	0.22 °C	-2.77 °C	4.38 °C	–

5.3 Measured Compressive Strength

The following graphs shown in Figure 5.2 were generated using the compressive strength values obtained from the ConReg 806 system based on the temperature measurements recorded by the installed sensors. As the slabs were cast under different environmental conditions, variations in strength development were observed between them.

The temperature sensors remained installed for varying durations depending on the slab. Since the casting took place during winter, between 31 October and 22 February, specific precautionary measures were implemented to ensure adequate curing conditions. A 1 cm thick expanded polyethylene (EPE) insulation layer was placed on top of each slab. In addition, the underside of the slabs was continuously heated. According to Nils Rasmark (personal communication, 2026), who was responsible for on-site supervision, the heating maintained a temperature approximately 5°C above the ambient air temperature throughout the curing period.

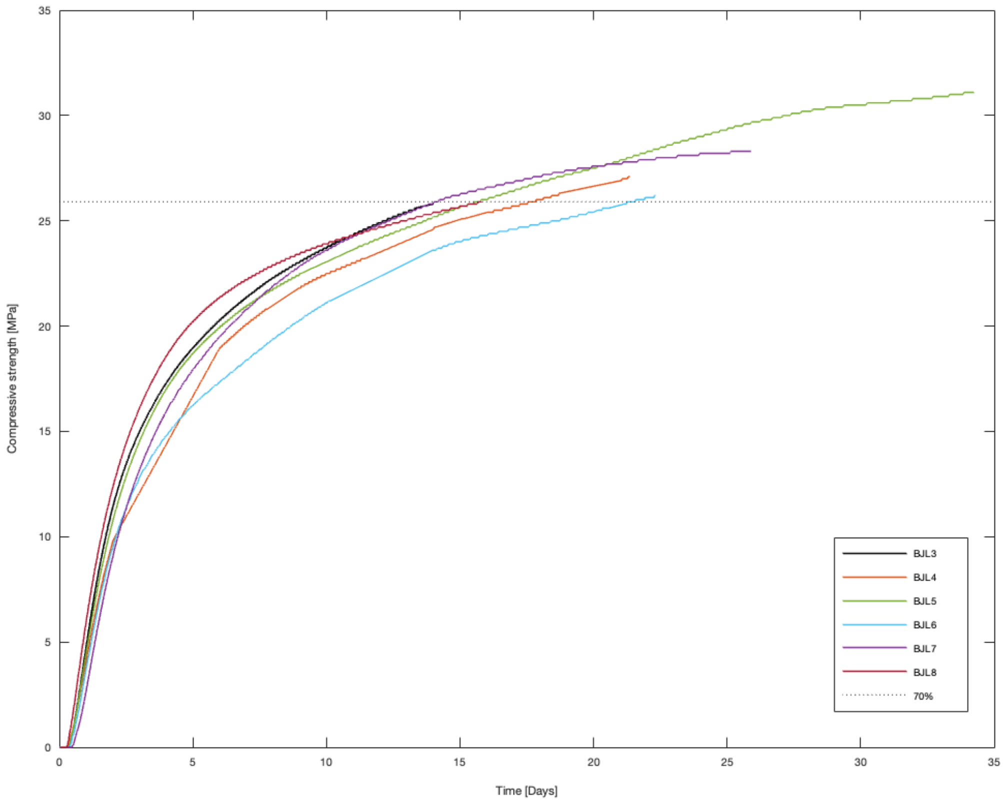

Figure 5.2: Compressive strength development for the investigated floor slabs (BJL3–BJL8) as a function of time. The horizontal reference line indicates 70% of $f_{c,cube}$

5.4 Calibration of Curing Model

In the PPB software, most predefined concrete mixes are primarily based on conventional cement compositions and therefore do not represent the high levels of slag replacement commonly used in climate-improved concretes. Through personal communication with Nils Rasmark, a mix design corresponding approximately to a Level 4 climate-improved concrete (see Table 2.5) was obtained and used as the initial input for the simulations. This reference mix is estimated to contain more than 32% ground granulated blast furnace slag (GGBS), although the exact slag content is not known.

The concrete investigated in this study, however, differs from the reference mix, as it contains 32% slag. While its exact classification within the Swedish climate levels is unknown, experimental data describing its strength development are available. Consequently, the initial PPB model based on a Level 4 concrete required calibration in order to represent the behavior of the studied concrete more accurately.

The calibration was performed by systematically modifying selected material parameters in the PPB model. Starting from the initial Level 4 mix, one parameter at a time was adjusted, and its influence on the simulated strength development was evaluated. The selection of parameters to adjust was guided by previous sensitivity and probabilistic studies, including Monte Carlo simulations (Hedlund et al., 1996), which identify the parameters with the greatest influence on temperature development, strength evolution, and cracking risk in early-age concrete.

By comparing the simulated strength development with the experimentally measured data for the 32% slag concrete, iterative adjustments were made to the model. This trial-and-error process allowed the identification of a parameter set that better reproduces the observed behaviour. The calibration was considered complete once a satisfactory agreement between simulated and measured strength development was achieved.

The resulting parameter set, together with the original Level 4-based input, is presented in Table 5.3. The table highlights the specific parameters that were modified during the calibration process and illustrates how the initial climate-improved concrete model was adapted to represent the studied concrete.

Table 5.3: Comparison of PPB input parameters: *Level 4 recipe* vs. *adjusted recipe*.

Parameter	**Level 4**	**Adjusted**
General		
Density (kg/m^3)	2350.0	2350.0
Heat capacity (J/(kg·K))	1000.0	1000.0
Heat development		
W_u (J/kg)	317000	317000
Λ_1 (-)	1.0000	1.0000
t_1 (h)	12.216	12.216
κ_1 (-)	1.215	1.215
Maturity and strength		
$t_{e,ini}$ (h)	7.00	9.00
$t_{e,fin}$ (h)	9.00	11.00
t_{e0} (h)	0.00	0.00
$\beta_{D,ini}$ (-)	1.0	1.0
$\Theta_{\text{ref},ini}$ (K)	4298	4250
$\kappa_{3,ini}$ (-)	0.192	0.300
s (-)	0.192	0.177
N_{set} (-)	3.000	3.200
N_{cc28d} (-)	0.694	0.600
$\beta_{D,set}$ (-)	1.0	1.0
$\Theta_{\text{ref},set}$ (K)	4298	4250
$\kappa_{3,set}$ (-)	0.192	0.300
$\beta_{D,fin}$ (-)	1.0	1.0
$\Theta_{\text{ref},fin}$ (K)	4298	4250
$\kappa_{3,fin}$ (-)	0.192	0.300
$F_{cc,set}$ (MPa)	0.5	0.5
Strength reduction due to high temperature		
DMaxDrop28d (-)	0.250	0.250
TempD (°C)	41.0	41.0
κ_{Temp} (-)	1.900	1.900
TimeD (h)	46.8	46.8
κ_{Time} (-)	1.900	1.900

The initial behaviour of the concrete model can be observed in Figure 5.3. The left curve represents the simulation using the original class 4 recipe, while the right curve shows the results obtained after calibration of the material parameters.

When comparing the simulated strength development for the Level 4 GGBS concrete with the strength evolution derived from the maturity function in the ConReg measurements, the difference is relatively small but still clearly noticeable. The original recipe shows a slower strength development during the early stages of hydration, followed by a slightly more pronounced increase at later ages.

Through calibration of the material parameters, the simulated curve was adjusted in order to better reproduce the measured strength development. The calibrated recipe therefore provides a more representative description of the investigated concrete, particularly during the early hardening phase where the difference between the simulations and the measurements was most pronounced.

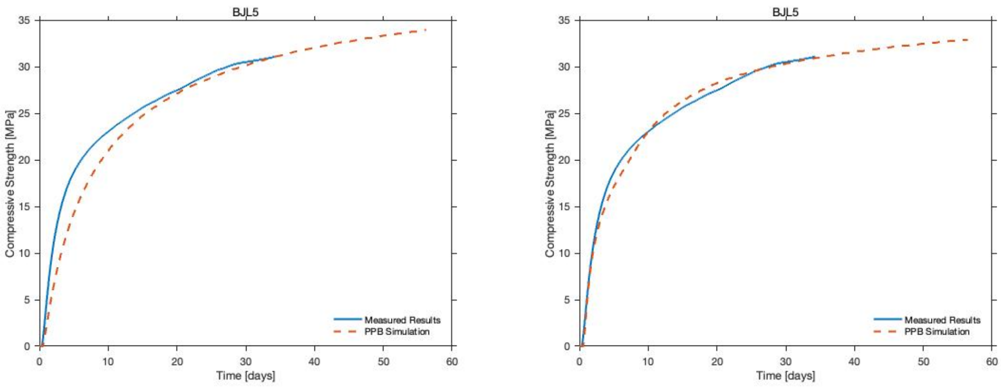

Figure 5.3: Comparison between the Level 4 and the new calibrated recipe for BJL5.

Following the comparison shown in Figure 5.3, several parameters in the PPB material model were adjusted in order to better reproduce the experimentally observed strength development.

The parameters $t_{e,ini}$ and $t_{e,fin}$ describe the early-age behaviour of the concrete and represent the transition from the fresh state to the hardening phase. These parameters were increased in order to better represent the delayed hydration typically observed in climate-improved concretes containing a high proportion of GGBS. Such concretes generally exhibit slower early-age reactions compared to conventional Portland cement concretes (Hedlund et al., 1996).

All κ parameters were also increased. These parameters govern the temperature sensitivity of the hydration rate and therefore control how strongly the hydration process responds to temperature variations. In the original recipe, the simulated strength development showed a relatively small response to changing temperature conditions compared to what could be observed in the measured data. Increasing the κ values therefore allowed the model to better capture the stronger temperature dependence observed in the real structure (Hedlund et al., 1996).

The shape parameter s was additionally adjusted. This parameter controls the overall form of the strength development curve and influences the rate of strength increase. A higher value of s typically results in a steeper increase in strength at later ages, while the initial part of the curve becomes somewhat flatter. Since the shape of the curve is closely related to the compressive strength at 28 days, this parameter often needs to be calibrated against experimental measurements. In practice, the measured 28-day strength may differ from the nominal strength class (e.g. C30/37), which means that the parameter must sometimes be adjusted to obtain a representative strength development curve (Hedlund et al., 1996).

To illustrate how these parameters were modified relative to the original high-slag recipe used as a starting point, the complete set of PPB input parameters is presented in Table 5.3.

5.5 Measured values compared with PPB

In order to reproduce the casting conditions as realistically as possible, the boundary conditions in the PPB simulations were adjusted to reflect the curing environment observed on site. During casting, the slabs were exposed to heating from below due to the underlying structure, while the top surface was covered with insulating blankets to reduce heat loss.

To account for this, the underside of the slabs was modelled using the boundary condition *weather protection* with an additional temperature increase of 5°C. This assumption was introduced to approximate the heating effect from the structure beneath the slab.

For the upper surface, a covering corresponding to *insulating blanket 1 cm* was applied in the PPB model in order to represent the thermal insulation used during curing on site. The duration of this covering was assumed to correspond to the period during which the slabs remained supported by temporary props. The applied durations for each slab are summarized in Table 5.4.

Table 5.4: Duration of slab covering corresponding to the period with temporary props in place.

Slab ID	Covering duration (days)
BJL3	14
BJL4	22
BJL5	15
BJL6	21
BJL7	22
BJL8	16

Using these calibrated material parameters, the same strength development model was then used to simulate the in-situ slabs. The slab geometry was modified to correspond to the actual casting configuration, and a weather file was created based on the recorded ambient temperatures presented in Table 4.1. Furthermore, the initial concrete temperature and the maximum measured concrete temperature were defined according to the recorded temperature data for each slab. The purpose of this comparison is to assess how well the calibrated PPB model reproduces the measured maturity-based strength development under realistic environmental conditions, and to evaluate the extent to which the program accounts for varying weather exposure.

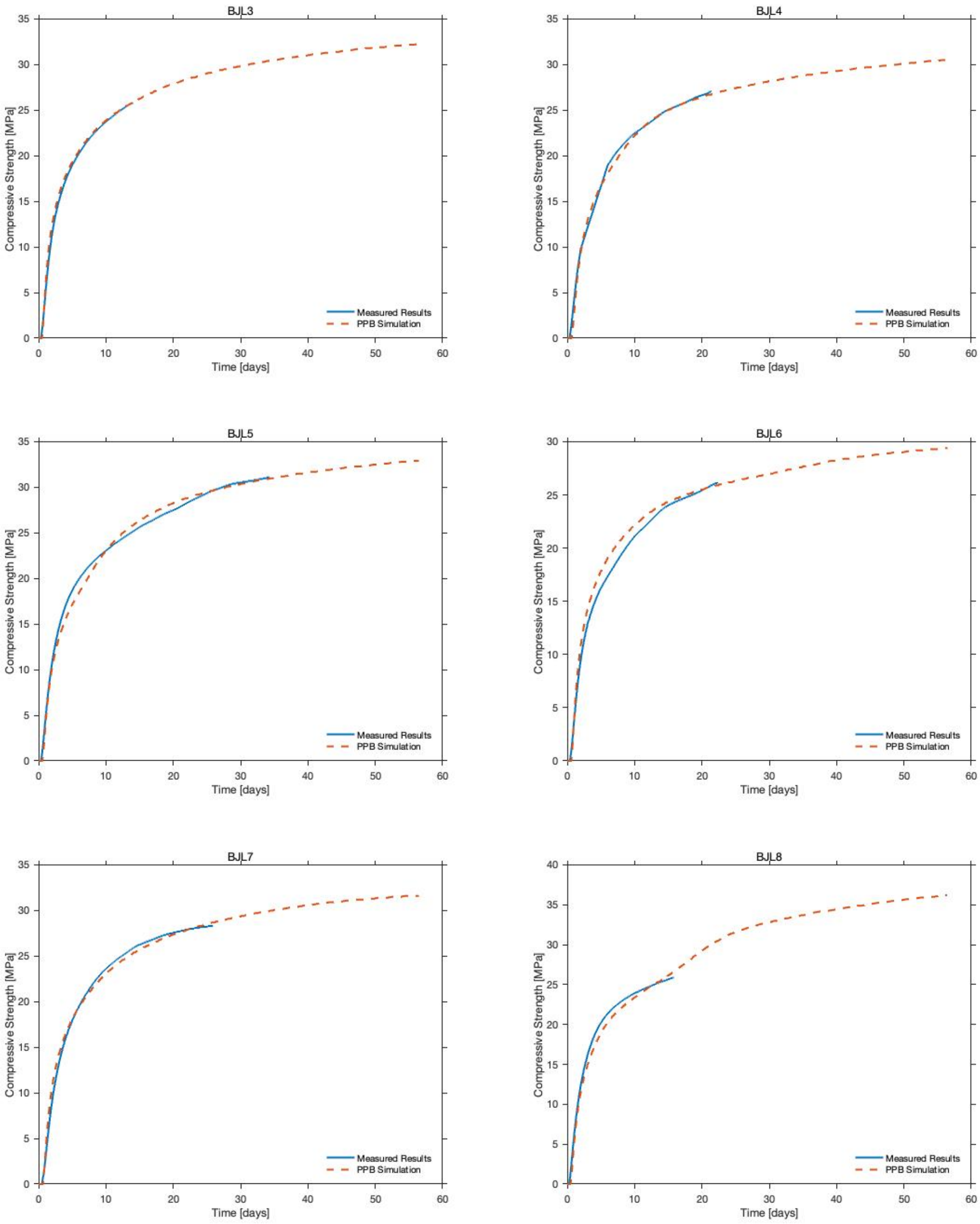

Figure 5.4: Comparison between PPB simulations and graphs based on measured temperatures.

The graphs indicate that the PPB model provides a reasonably accurate estimation of the strength development for the investigated slabs. In general, the simulated curves follow the same overall trend as the strength development derived from the maturity calculations.

It should be noted that the temperature measurements for all slabs were terminated before the full 56-day period simulated in PPB. Consequently, the maturity-based strength development derived from measurements is only available up to the respective monitoring end date, whereas the PPB simulations continue beyond this point.

This limitation is particularly relevant for slab BJL8. The climatic input used in PPB was defined in discrete time intervals, as only weekly ambient temperature data were available. This results in stepwise changes in the applied temperature history. For example, in the PPB input for BJL8 the ambient temperature changes abruptly from approximately -2°C to 4.5°C between two consecutive days, whereas in reality such a temperature increase would likely have occurred gradually over several days.

Since the temperature measurements were terminated before the end of the simulated period, the later part of the PPB simulations cannot be directly verified against measured data. In addition, the climatic input in PPB was defined using weekly average temperatures, which results in stepwise changes in the applied temperature history. In reality, such temperature variations would likely occur more gradually. Consequently, the simulated strength development after the monitoring period, particularly for BJL8, should be interpreted with some caution.

5.5.1 Estimated strength gain

To facilitate a clearer comparison between the different slabs, the maturity-based compressive strength at 28 and 56 days was extracted from the recorded temperature histories. The results are summarised in Table 5.5.

The table presents the estimated compressive strength at both ages together with the absolute and relative strength increase between 28 and 56 days. This provides an overview of how the in-situ slabs developed strength over time and allows the long-term strength development to be compared between the different casting conditions.

Table 5.5: Summary of maturity-based strength development for the monitored slabs between 28 and 56 days.

	BJL3	**BJL4**	**BJL5**	**BJL6**	**BJL7**	**BJL8**
$f_{c,28}$ (MPa)	29.5	27.9	30.1	26.7	29.1	32.4
$f_{c,56}$ (MPa)	32.2	30.5	32.9	29.4	31.6	36.2
$\Delta f_{28\to 56}$ (MPa)	2.7	2.6	2.8	2.7	2.5	3.8
$\Delta f_{28\to 56}$ (%)	9.2	9.3	9.3	10.1	8.6	11.7

As shown in Table 5.5, the estimated increase in compressive strength between 28 and 56 days ranges from approximately 2.5 to 3.8 MPa, corresponding to a relative increase of about 8.6 to 11.7%. This continued strength development beyond 28 days is consistent with the delayed hydration behaviour typically observed in concretes containing GGBS.

5.6 Comparison Between Laboratory Results and PPB Simulations

The purpose of this comparison is to evaluate the model's capability to reproduce the observed later-age strength development for slag-containing concretes.

5.6.1 PPB Laboratory Model

In order to recreate the laboratory test conditions, a 2D cross-section representing a concrete cube with dimensions 150 × 150 mm was modeled in PPB. The ambient air temperature was set to 20°C, and all surfaces were exposed to heavy wind conditions (approximately 12 m/s). The temperature of the fresh concrete mixture was also set to 20°C.

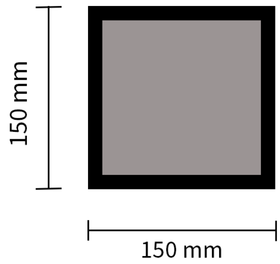

Figure 5.5: Geometry of the modeled 150 × 150 × 150 mm test cube used for laboratory simulation in PPB.

The numerical model was established to replicate the thermal and environmental conditions of the laboratory tests as closely as possible. By modelling a cube with identical geometry and subjecting it to constant boundary conditions of 20°C, the simulation aimed to reproduce the controlled curing environment used in the experimental program. The assumption of heavy wind exposure on all surfaces was introduced to ensure efficient convective heat transfer, thereby approximating the relatively uniform temperature conditions typically maintained in laboratory storage. By maintaining identical initial concrete temperature and ambient conditions, the model isolates the influence of hydration kinetics and material parameters on strength development. This setup enables a direct comparison between experimentally measured compressive strengths and the strengths predicted by the PPB model.

5.6.2 The predictive capability of the model for different slag levels

The calibrated PPB recipe was established using the measured strength development of the reference slab concrete, which had a GGBS replacement level of 32%. The purpose of this calibration was therefore to obtain a material model that reproduces the behaviour of this specific reference concrete as closely as possible.

After the calibration, this material model was used as a reference model in the comparison with the laboratory concrete mixes. In these simulations, only the basic mix-related input parameters such as water–cement ratio, strength class and binder content were adjusted to reflect the laboratory mixtures. The calibrated material parameters governing the hydration and strength development were otherwise kept unchanged.

It should therefore be emphasized that the comparisons presented in this section do not represent a separate calibration for each laboratory mix. Instead, they are intended to evaluate to what extent a material model calibrated for a concrete with approximately 32% GGBS can also provide a reasonable estimate of the strength development for concretes with different water–cement ratios, strength classes and slag contents.

Since PPB does not allow the slag content to be modified directly through a single dedicated parameter, the influence of slag content is only reflected indirectly through the calibrated material model. The purpose of the comparison is thus not to claim that the model exactly represents each laboratory mix, but rather to assess whether the calibrated recipe can be regarded as approximately representative across a wider range of slag-containing concretes. The resulting strength development curves are presented below.

Figures 5.6–5.8 show the comparison between the experimentally obtained cube compressive strength values and the simulated strength development predicted by the PPB model.

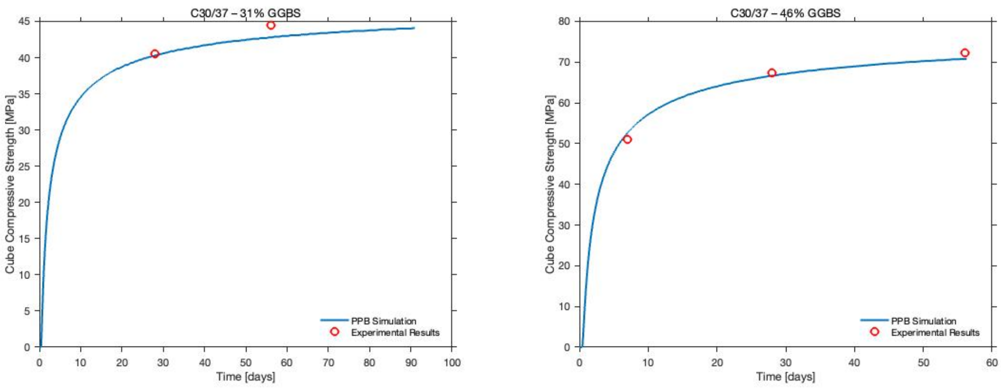

Figure 5.6: Comparison of strength development for C30/37 concrete with 31% and 46% GGBS.

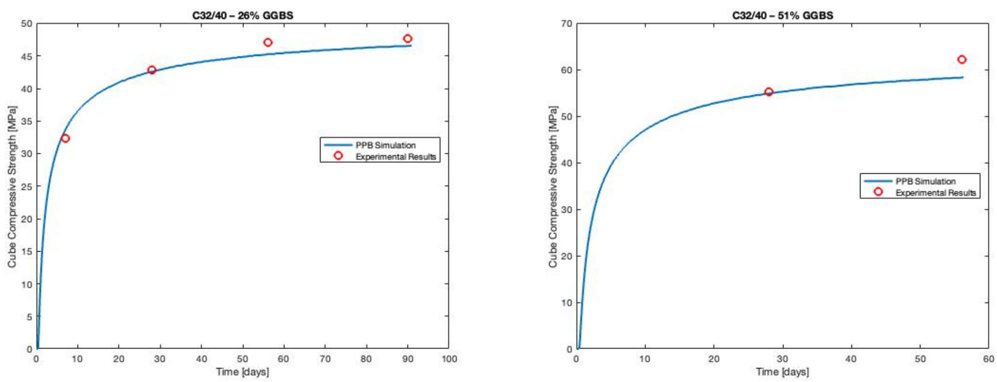

Figure 5.7: Comparison of strength development for C32/40 concrete with 26% and 51% GGBS.

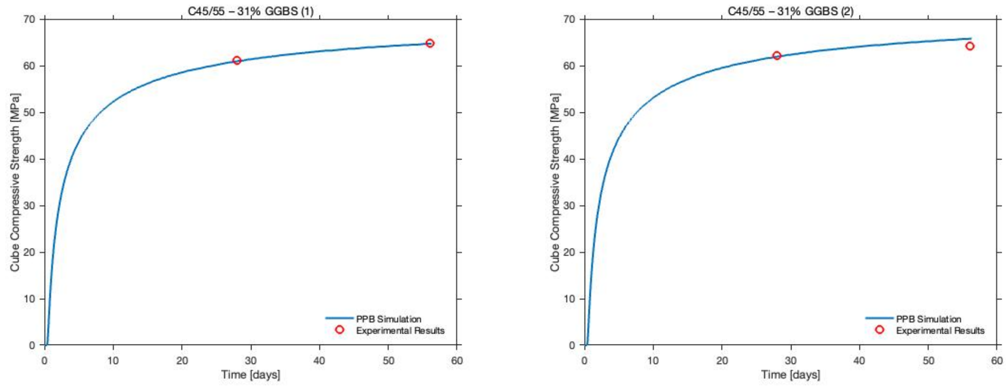

Figure 5.8: Comparison of strength development for C45/55 concrete with 31% GGBS (two laboratory series).

Furthermore, the strength values obtained from both the laboratory experiments and the PPB simulations have been compiled in Table 5.6. The table summarises the input parameters together with the compressive strength at 28 and 56 days, as well as the corresponding strength increase over this period for both the experimental results and the PPB predictions.

Table 5.6: Summary of input parameters and comparison between laboratory results and PPB predictions (28–56 days).

Parameter	C32/40 26% GGBS	C32/40 51% GGBS	C45/55 31% GGBS (1)	C45/55 31% GGBS (2)	C30/37 31% GGBS	C30/37 46% GGBS
Input data						
w/c (vct)	0.55	0.50	0.40	0.40	0.55	0.55
GGBS content (% of binder)	26%	51%	31%	31%	31%	46%
Laboratory results						
$f_{c,28}$ (MPa)	42.8	55.2	61.3	62.3	40.5	67.3
$f_{c,56}$ (MPa)	47.1	62.2	64.9	64.3	44.5	72.4
$\Delta f_{28\to56}$ (MPa)	4.3	7.0	3.6	2.0	4.0	5.1
$\Delta f_{28\to56}$ (%)	10.05%	12.68%	5.87%	3.21%	9.88%	7.58%
PPB prediction						
$f_{c,28}$ (MPa)	42.8	55.2	61.3	62.3	40.5	67.3
$f_{c,56}$ (MPa)	45.3	58.4	64.8	65.9	42.8	70.8
$\Delta f_{28\to56}$ (MPa)	2.5	3.2	3.5	3.6	2.3	3.5
$\Delta f_{28\to56}$ (%)	5.84%	5.80%	5.71%	5.78%	5.68%	5.20%

From Table 5.6 it can be observed that the PPB simulations consistently predict a strength increase of approximately 5–6% between 28 and 56 days.

In contrast, the laboratory results show a larger variation, with the corresponding increase ranging from about 3% to 13%, and an average value of approximately 8%.

Table 5.7: Difference between laboratory results and PPB predictions (Lab – PPB).

Metric	C32/40 26%	C32/40 51%	C45/55 31% (1)	C45/55 31% (2)	C30/37 31%	C30/37 46%
$\Delta f_{c,56}$ (MPa)	1.8	3.8	0.1	-1.6	1.7	1.6
$\Delta(\Delta f_{28\to56})$ (pp)	4.21	6.88	0.16	-2.57	4.20	2.38

Table 5.7 presents the difference between the laboratory measurements and the PPB predictions. The first row shows the difference in compressive strength at 56 days, calculated as the laboratory value minus the PPB prediction. Positive values therefore indicate that the PPB model underestimates the compressive strength, while negative values indicate that the model overestimates it.

The second row presents the difference in the relative strength increase between 28 and 56 days, expressed in percentage points. This metric illustrates how well the model captures the long-term strength development compared to the laboratory results. As shown in Table 5.7, the PPB model underestimates the 56-day compressive strength in the majority of the analysed cases. As shown in Table 5.7, the PPB model underestimates the 56-day compressive strength in the majority of the analysed cases. The largest deviation is observed for the concrete mixture with the highest GGBS content.

This behaviour is likely related to the calibration of the material model, which was primarily adjusted to match a concrete mixture containing approximately 32% GGBS. As a result, the model tends to overestimate the early-age strength development for mixtures with higher slag content, while simultaneously underestimating the long-term strength gain.

6 Application of Calibrated Model at Building Scale

6.1 Analysis of Existing Building

An existing residential building has been used as a reference case in this study. The geometry and structural conditions of the building serve as a basis for the analyses presented in the following sections.

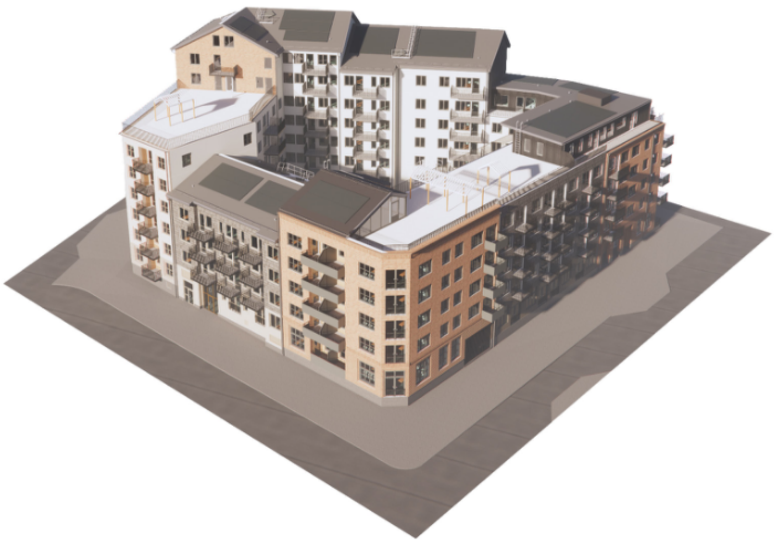

Figure 6.1: Reference building used for the case study analysis.

The purpose of this analysis is to compare the strength development of concrete elements produced with and without GGBS, and to assess whether a reduction in strength class is feasible when using GGBS-based concrete, while still achieving a 56-day compressive strength equivalent to the 28-day strength of the higher class.

In the PPB simulations, the 28-day compressive strength is set equal to the characteristic cube strength of the specified strength class. For C30/37, this corresponds to 37 MPa at 28 days, meaning that the concrete is assumed to just satisfy the minimum requirement for its strength class. In practice, the mean strength of delivered concrete typically exceeds the characteristic value, as the characteristic strength represents the 5th percentile of the strength distribution. The simulations therefore represent a conservative lower bound for the strength development.

The strength reported for each structural element corresponds to the average compressive strength across the cross-section. Since temperature gradients develop during hydration, the strength development may differ marginally between the top, middle and bottom of the element. The average value is considered representative for the purpose of this comparison.

Weather data

The environmental boundary conditions used in the simulations were based on measured air temperature data obtained from the Swedish Meteorological and Hydrological Institute (SMHI). The data were collected from an active weather station located in Gothenburg, station ID 71420 (SMHI, 2026).

The selected time period corresponds to April–June 2025 and was chosen to represent typical curing conditions during spring in Gothenburg. The temperature data were processed and used to define the external climate conditions in the PPB simulations. The temperature was input at 6-hour intervals, corresponding to four measurements per day at 00:00, 06:00, 12:00, and 18:00.

Wind conditions were also considered based on data from the same weather station. The measured mean wind speed during the selected period was approximately 3.2 m/s. As PPB only allows predefined wind categories, the boundary condition corresponding to moderate wind (6 m/s) was applied, as it was considered to best represent the overall exposure conditions.

6.2 Filigree floor slab

The studied building includes a filigree floor slab with a concrete strength class of C30/37. The exposure class was assumed to be X0, which corresponds to concrete not exposed to corrosion risk or other environmental attack (Svenska Betongföreningen, 2009).

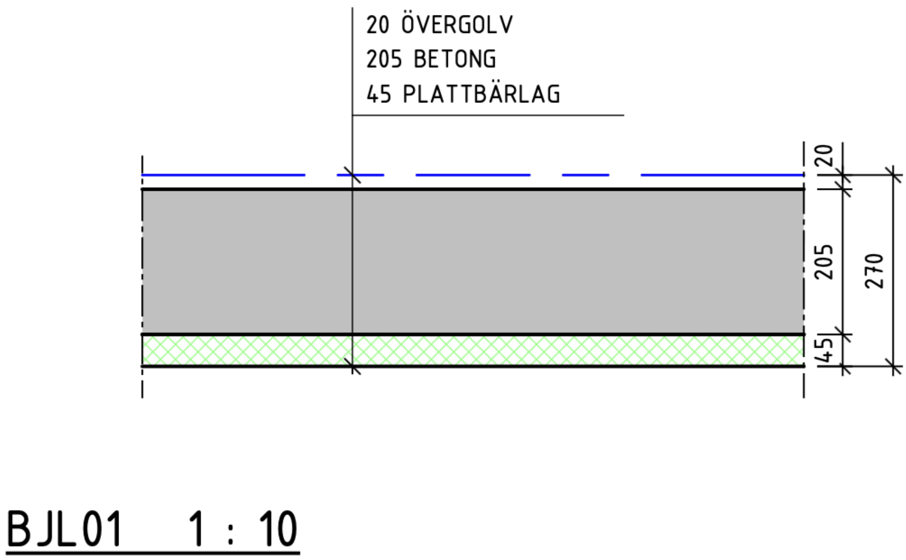

Figure 6.2: Dimensions of the reference floor slab.

The filigree floor slabs act as permanent formwork for the in-situ cast concrete. The initial temperature of the fresh concrete was assumed to be 20°C, while the temperature of the precast concrete was set to 10°C.

The underside of the slab was assumed to be exposed, as the lattice girders are in direct contact with the supporting structure and no thermal protection is present. The top surface was assumed to be covered after casting using plastic sheeting for a duration of seven days, in order to reduce moisture loss and support curing conditions.

Simulation results

When simulating, three different scenarios were chosen and then compared, namely, using Portland cement, using the calibrated 32% GGBS approximation and finally lowering the compressive strength one level to C28/35 with the same 32% GGBS concrete. These simulations are plotted in figure 6.3.

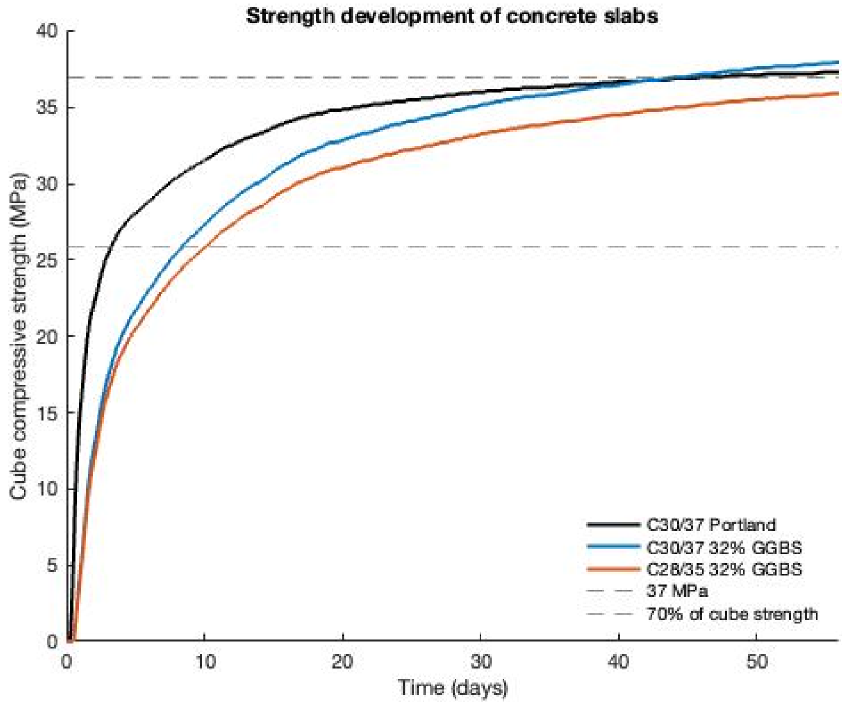

Figure 6.3: Simulated strength development for the filigree floor slab

Table 6.1: Summary of strength development for the analysed slab concretes. The age at which 70% of 37 MPa is reached corresponds to 25.9 MPa.

Parameter	C30/37 Portland	C30/37 32% GGBS	C28/35 32% GGBS
Age at 25.9 MPa (days)	2.67	7.63	9.25
$f_{c,28}$ (MPa)	36.0	35.0	33.1
$f_{c,56}$ (MPa)	37.4	38.2	36.1
$\Delta f_{28\rightarrow 56}$ (MPa)	1.4	3.2	3.0
$\Delta f_{28\rightarrow 56}$ (%)	3.9%	9.1%	9.1%

The results presented in Table 6.1 show that the C28/35 concrete with 32% GGBS reaches a compressive strength of 36.1 MPa at 56 days, which falls marginally short of the 37 MPa cube strength associated with C30/37. Given that strength development has not yet plateaued at this age, it is reasonable to expect that this threshold will be reached at a slightly later age.

A clear difference in strength gain between the Portland cement concrete and the GGBS mixes is also evident. While the Portland reference exhibits an increase of only 3.9% between 28 and 56 days, both GGBS mixes show an increase of approximately 9%, consistent with the more pronounced later-age strength development of slag-containing concretes discussed in Section 2.1.2. The delayed early-age strength development is also reflected in the time required to reach 25.9 MPa, corresponding to 70% of the C30/37 cube strength, which increases from 2.67 days for Portland cement to 7.63 and 9.25 days for the C30/37 and C28/35 GGBS mixes respectively.

6.3 Ground slab

The ground slab is modelled as a slab cast directly on the ground, without piling. The geometry is based on the reference building and the dimensions shown in Figure 6.4. The concrete strength class was assumed to be C30/37.

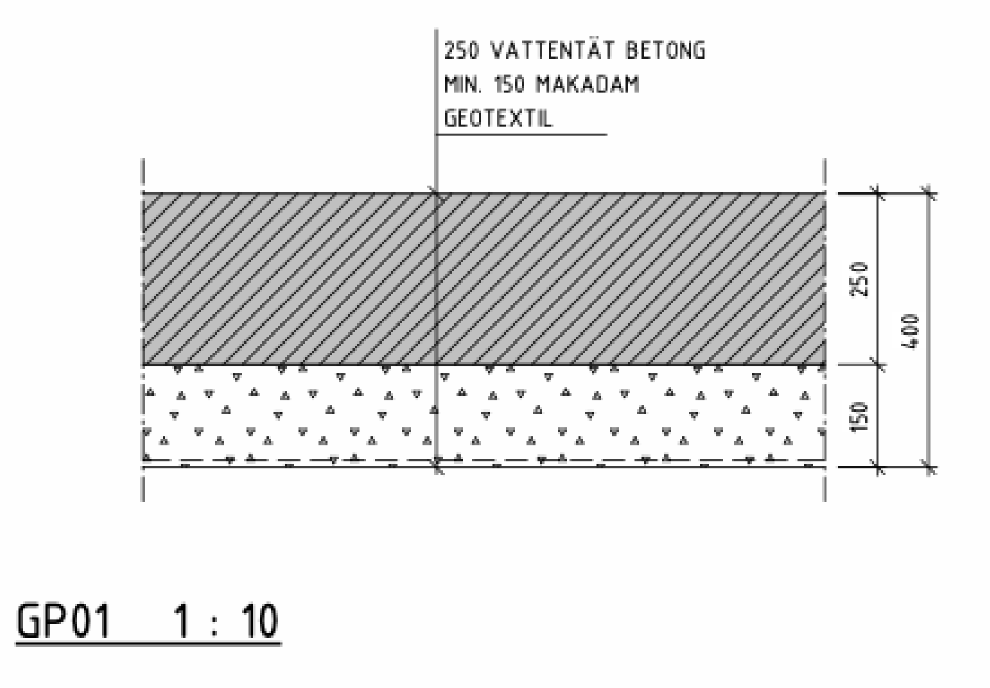

Figure 6.4: Dimensions of the ground slab.

The ground slab was assumed to be in contact with the soil and was therefore assigned exposure class XC2 which is typical for construction parts that are wet and rarely dry. Since PPB does not provide a specific option for crushed rock or macadam, the supporting layer was approximated as gravel/moraine, which was considered to best represent the thermal behaviour of the foundation material.

The initial ground temperature was assumed to be 10°C. This value was selected to represent a temperature slightly lower than the mean air temperature during the studied period, which was approximately 13°C according to the weather data. The initial temperature of the fresh concrete was set to 20°C.

No weather protection was assumed during casting. However, the slab was assumed to be covered with plastic sheeting after casting in order to reduce moisture loss during curing. The formwork was modelled as 15 mm plywood.

As the calibrated material model is based on a concrete with a water-to-binder ratio of 0.55, the ground slab was simulated using the C30/37 concrete with the same water-to-binder ratio. Although lower strength classes are often associated with higher water-to-binder ratios in practice, this parameter could not be varied within the scope of the calibrated model. The comparison should therefore be understood as being based on a constant water-to-binder ratio.

Curing was assumed to continue until the concrete had reached 70% of the characteristic cube compressive strength, after which construction activities on the slab were assumed to commence.

Simulation results

When simulating the ground slab the following results can be seen for the three different mixes as seen in 6.5.

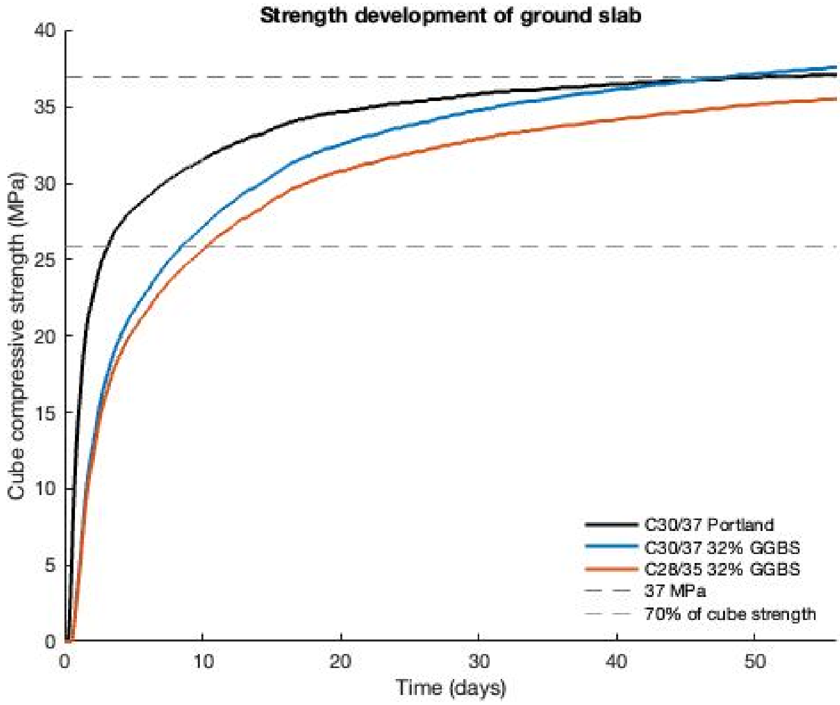

Figure 6.5: Simulated strength development for the ground slab.

Parameter	C30/37 Portland	C30/37 32% GGBS	C28/35 32% GGBS
Age at 25.9 MPa (days)	2.54	7.83	9.67
$f_{c,28}$ (MPa)	35.7	34.4	32.6
$f_{c,56}$ (MPa)	37.2	37.7	35.6
$\Delta f_{28\to56}$ (MPa)	1.5	3.3	3.0
$\Delta f_{28\to56}$ (%)	4.2%	9.6%	9.2%

Table 6.2: Strength development for the ground slab.

As in the suspended slab simulations, the climate-reduced concretes show a clearly larger increase in strength between 28 and 56 days than the Portland concrete. The same general trend is therefore observed for both structural elements.

At the same time, the delayed early-age strength development is more pronounced for the ground slab than for the suspended slab. This can be explained by the thermal boundary conditions, the ground slab is cast directly against cooler soil, which increases heat loss through the bottom surface and lowers the internal temperature during the early hydration phase. Since slag-containing concretes are more sensitive to temperature than Portland cement concrete, this results in a more pronounced delay in early strength gain. The insulating effect of the greater slab thickness partially counteracts this, as it reduces heat dissipation through the top surface, but the dominant effect is the heat loss to the colder supporting ground.

It should be noted that C28/35 with 32% GGBS does not reach 37 MPa at 56 days under the simulated conditions. However, simulations extended to 90 days indicate that this strength level is reached at approximately 84 days. However, the strength which the C28/35 has reached after 56 days is similar to the one which the Portland cement has reached after 28 days.

6.4 Basement wall

The basement wall model is based on the geometry of the studied building. The wall has a thickness of 250 mm and is assumed to be cast on the ground slab, with a strength class of C30/37 and an exposure class of XC2. During casting, the excavation is assumed to be open on both sides of the wall, meaning that both wall surfaces are exposed to ambient outdoor conditions during the early construction stage.

The ground surface temperature was assumed to be 10°C, while the temperature within the surrounding soil mass was set to 7°C. The wall was assumed to stand directly on the ground slab, allowing heat transfer between the two structural elements.

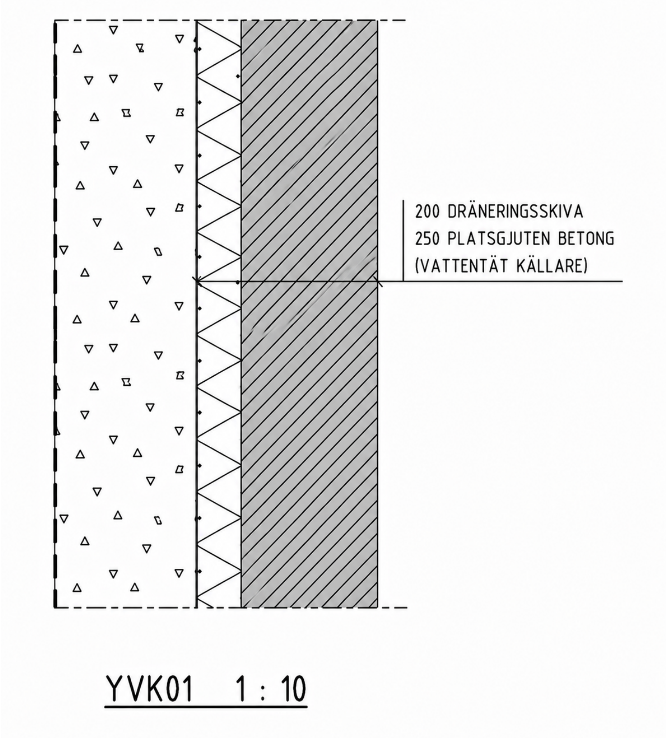

Figure 6.6: Basement wall geometry based on the reference building.

Where the basement wall exceeds over the surface the exterior is covered with 100mm of insulation followed by an air cavity and then a 120mm prefabricated concrete element, as seen in figure 6.6. Because of this the concrete falls into exposure category XC2.

The assumptions regarding formwork removal were made based on the practical objective of removing the formwork as early as possible, since prolonged formwork retention increases construction cost and reduces production efficiency. In the simulations, the formwork was therefore assumed to remain in place until the concrete reached a compressive strength of 5 MPa. After form removal, a vapour-tight plastic sheet was assumed to be applied within one hour in order to maintain curing.

The curing period was then assumed to continue until the concrete reached 35% of its 28-day characteristic cube compressive strength, in accordance with the curing requirements discussed previously. The required curing duration therefore varies depending on the simulated strength development of each concrete mixture.

Simulation results

When simulating the basement wall the following results can be seen for the three different mixes as seen in 6.7.

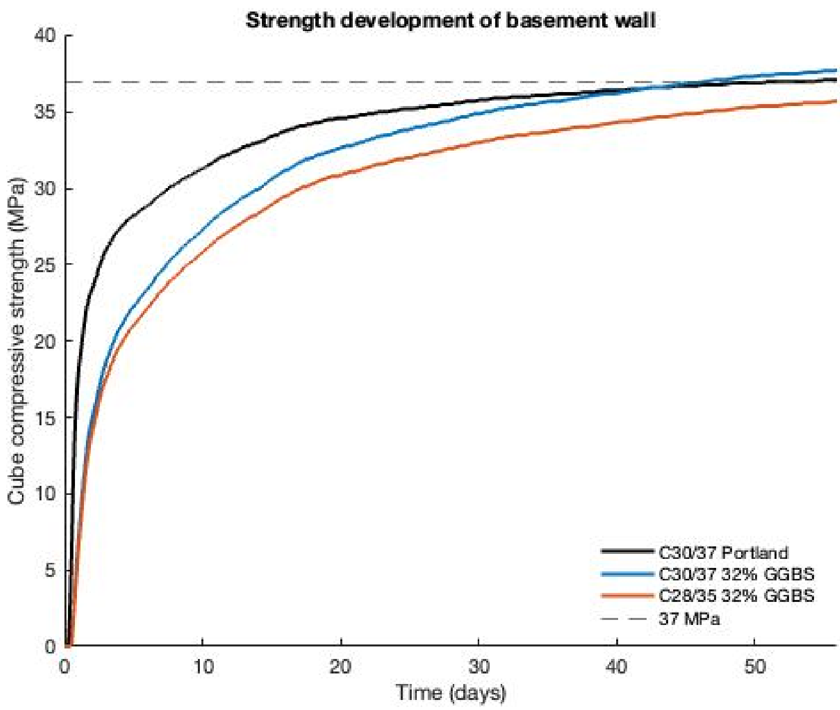

Figure 6.7: Simulation results PPB

The difference between the different strength classes of GGBS concrete is the largest here. Furthermore the age when the form could be taken down, 5 MPa, was summarized in a table togheter with the age when the concrete reached 35% of the $f_{ck,cube}$. These are important from a production standpoint.

Parameter	**C30/37 Portland**	**C30/37 32% GGBS**	**C28/35 32% GGBS**
Age at 5 MPa (hours)	11	21	22
Age at 35% of $f_{ck,\text{cube}}$ (hours)	17	40	43
$f_{c,28}$ (MPa)	36.0	33.0	31.9
$f_{c,56}$ (MPa)	37.2	37.8	35.7
$\Delta f_{28\rightarrow 56}$ (MPa)	1.2	4.8	3.8
$\Delta f_{28\rightarrow 56}$ (%)	3.3%	14.5%	11.9%

Table 6.3: Early-age and long-term strength development for the basement wall.

Although the basement wall exhibited the largest strength increase between 28 and 56 days, this is mainly explained by its lower strength level at 28 days. In other words, the wall had a more delayed early-age strength development, leaving a greater potential for continued strength gain during the later curing period.

6.5 Reinforcement Demand — Floor Slab

This section investigates the reinforcement demand for a semi-precast floor slab using three approaches: minimum reinforcement for crack width control, ULS bending verification, and SLS deflection control. By comparing these approaches, it is possible to identify which limit state governs the reinforcement design and to assess the influence of concrete strength class on the required reinforcement.

The study is performed on a representative unit strip with a width of $b = 1000$ mm and a total thickness of $h = 250$ mm, consisting of a 50 mm filigree slab and a 200 mm in-situ concrete topping, in accordance with Thomas Betong AB (2016). All geometric and detailing parameters are kept constant while only the concrete strength class is varied.

6.5.1 Minimum Reinforcement for Crack Control

If all parameters except the concrete strength class are kept constant, an increase in strength class implies an increase in the required minimum reinforcement. In Eurocode 2, minimum reinforcement for crack control is derived from equilibrium at first cracking, where the tensile force carried by the concrete just before cracking is balanced by the force that the reinforcement can carry immediately after cracking. This is expressed as (SIS – Swedish Institute for Standards, 2005):

$$A_{s,\min}\,\sigma_s = k_c\,k\,f_{ct,eff}\,A_{ct}, \tag{6.1}$$

where $A_{s,\min}$ is the minimum reinforcement area, σ_s is the steel stress assumed at crack formation, A_{ct} is the effective tensile area of concrete, and k and k_c are coefficients accounting for stress distribution and the effect of self-equilibrating stresses, respectively. Rearranging Eq. (6.1) gives:

$$A_{s,\min} = \frac{k_c\,k\,f_{ct,eff}\,A_{ct}}{\sigma_s}. \tag{6.2}$$

The effective tensile area A_{ct} is conservatively assumed as half of the cross-section. The coefficient k is interpolated based on the section height in accordance with EKS 12. The effective tensile strength $f_{ct,eff}$ is set equal to f_{ctm}, and the steel stress σ_s is taken equal to the yield strength f_{yk}. Since only $f_{ct,eff}$ varies with concrete class while all other parameters remain constant, $A_{s,\min}$ increases in proportion to f_{ctm}, which itself increases with f_{ck} (SIS – Swedish Institute for Standards, 2005). The resulting minimum reinforcement areas are presented in Table 6.4.

Table 6.4: Minimum reinforcement demand for a 1000 mm wide, $h = 250$ mm semi-precast slab strip for varying concrete strength class.

Concrete strength class	$A_{s,\min}$ **[mm²/m]**
C20/25	188
C25/30	223
C28/35	240
C30/37	249
C35/45	274
C40/50	300
C45/55	326
C50/60	352

6.5.2 ULS Bending Verification

The minimum reinforcement requirements from crack width control are subsequently compared with the reinforcement demand from ULS bending verification. The same slab strip is modelled as a simply supported beam in StruSoft Concrete Beam, where the reinforcement is determined based on the design bending moment from uniformly distributed loads. A concrete density of 2500 kg/m^3 is adopted. The characteristic loads and corresponding design values are summarised in Table 6.5.

Table 6.5: Loads and partial safety factors used in ULS.

Load type	q_k **[kN/m^2]**	γ	$q_d = \gamma q_k$ **[kN/m^2]**
Imposed load (q_k)	2.00	1.50	3.00
Filigree slab self-weight ($g_{k,1}$)	1.25	1.35	1.69
In-situ concrete topping ($g_{k,2}$)	4.91	1.35	6.62
Sum permanent loads (g_d)			8.31
Total ULS load ($g_d + q_d$)			11.31

Simulations are performed for spans ranging from 5 m to 10 m and for concrete strength classes C25/30 to C40/50. The resulting required tensile reinforcement areas are presented in Table 6.6.

Table 6.6: Required tensile reinforcement area A_s [mm^2/m] from ULS bending verification in StruSoft for different spans and concrete strength classes.

Concrete class	**5 m**	**6 m**	**7 m**	**8 m**	**9 m**	**10 m**
C25/30	380	553	763	1013	1307	1652
C30/37	373	542	746	986	1267	1592
C35/45	372	540	741	979	1254	1571
C40/50	372	538	738	973	1245	1556

The results show that the concrete strength class has only a minor influence on the required reinforcement in ULS. Flexural resistance is primarily governed by the tensile reinforcement, while the concrete mainly carries compressive stresses. Increasing the concrete strength slightly reduces the depth of the compression zone and increases the internal lever arm, but this effect is small for typical slab sections. Furthermore, for all investigated spans the ULS reinforcement demand exceeds the minimum reinforcement from crack width control, indicating that ULS governs the reinforcement design in all cases.

6.5.3 SLS Verification

Although ULS governs the reinforcement demand, serviceability limit state criteria must also be verified. A SLS deflection control is therefore performed.

Deflections are evaluated under the quasi-permanent load combination, which includes all permanent loads and a fraction of the imposed load reduced by the quasi-permanent factor ψ_2. The loads used in the SLS analysis are summarised in Table 6.7.

Table 6.7: Loads and combination factors used in the quasi-permanent SLS combination.

Load type	F_k **[kN/m]**	**Coefficient**	F_{SLS} **[kN/m]**
Imposed load (Q_k), quasi-permanent	2.00	$\psi_2 = 0.30$	0.60
Filigree slab self-weight ($G_{k,1}$)	1.25	1.00	1.25
In-situ concrete topping ($G_{k,2}$)	4.91	1.00	4.91
Sum permanent loads (G_k)			6.16
Total quasi-permanent load			6.76

Long-term effects are accounted for by including creep and shrinkage parameters derived for the specific cross-section. The notional size is calculated as:

$$h_0 = \frac{2A_c}{u} = \frac{2 \times 250\,000}{1000} = 500 \text{ mm} \tag{6.3}$$

Where only the top surface is assumed to be exposed to drying, as the bottom is protected by the filigree slab. Assuming $t_0 = 28$ days and $RH = 50\%$, the creep coefficients for the different concrete strength classes are calculated and presented in Table 6.8.

Table 6.8: Creep coefficients $\varphi(t, t_0)$ for varying concrete strength classes. $RH = 50\%$, $t_0 = 28$ days, $h_0 = 500$ mm.

	C25/30	**C30/37**	**C35/45**	**C40/50**
f_{ck} (MPa)	25	30	35	40
f_{cm} (MPa)	33	38	43	48
φ_{RH}	1.63	1.63	1.63	1.63
$\beta(f_{cm})$	2.93	2.73	2.56	2.42
$\beta(t_0)$	0.485	0.485	0.485	0.485
$\varphi(t, t_0)$	2.291	2.055	1.827	1.648

Shrinkage is divided into drying shrinkage and autogenous shrinkage according to Eq. (.15). Drying shrinkage is assumed to commence at $t_s = 7$ days, corresponding to the time at which the formwork is typically removed and the surface becomes exposed to the surrounding environment. The resulting total shrinkage strains are presented in Table 6.9. The creep and shrinkage parameters have been determined using the built-in calculation tools in StruSoft Concrete Beam. The corresponding calculation procedure is presented in Appendix C.

Table 6.9: Total shrinkage strain ε_{cs} for varying concrete strength classes. $RH = 50\%$, $t = 18\,250$ days, $t_s = 7$ days, $h_0 = 500$ mm.

	C25/30	**C30/37**	**C35/45**	**C40/50**
ε_{cs} (‰)	0.320	0.314	0.310	0.307

The deflection limit used is $L/250$, which represents the maximum allowable total long-term deflection under quasi-permanent loading (SIS – Swedish Institute for

Standards, 2005). The reinforcement used in each deflection analysis corresponds to the minimum value obtained from the ULS bending verification for the respective span and concrete class. The computed long-term deflections for 6 m and 7 m spans are presented in Tables 6.10 and 6.11.

Table 6.10: Long-term deflection including creep and shrinkage for a 6 m span.

Concrete class	Deflection [mm]	$L/250$ [mm]	Status
C25/30	18.59	24	✓
C30/37	7.20	24	✓
C35/45	6.51	24	✓
C40/50	5.96	24	✓

Table 6.11: Long-term deflection including creep and shrinkage for a 7 m span.

Concrete class	Deflection [mm]	$L/250$ [mm]	Status
C25/30	38.69	28	×
C30/37	35.32	28	×
C35/45	30.50	28	×
C40/50	25.51	28	✓

The results indicate that deflection is not a governing criterion for spans up to 6 m, where all strength classes satisfy $L/250$ with sufficient margin. However, for a 7 m span most of the investigated concrete classes exceed the deflection limit when reinforced according to the ULS demand, suggesting that deflection governs the design at this span length regardless of concrete strength class. The notable difference in deflection between C25/30 and the higher strength classes at 6 m is attributed to cracking behaviour: C25/30 has a lower tensile strength f_{ctm}, making the cross-section more susceptible to cracking under the applied loads, which significantly reduces the effective stiffness and increases deflection.

6.6 Reinforcement Demand — Basement Wall and Ground Slab

Both the ground slab and the basement external wall share similar exposure conditions: both elements are in contact with soil and subjected to moisture from one side, with the ground slab exposed to water pressure from below and the basement wall exposed to lateral earth and water pressure. For both elements, the reinforcement demand is assumed to be governed by crack width control, which is directly dependent on the concrete strength class through the tensile strength f_{ctm}. This is in contrast to the floor slab, where ULS bending governs and the influence of strength class is marginal.

For the basement wall, only the horizontal reinforcement is investigated, as the vertical reinforcement is assumed to be governed by external loads, which as shown previously are only marginally affected by the concrete strength class. The purpose of this section is therefore to quantify the minimum reinforcement required for crack width control across different strength classes, and to assess how the reinforcement demand changes when the strength class is varied.

Both elements are assumed to have a thickness of 250 mm and the analysis is carried out on a 1000 mm wide strip. A double-reinforced cross-section is assumed.

Both elements are assumed to be thermally insulated, and a relative humidity of RH = 55% is therefore adopted. To account for uncertainties in the shrinkage prediction, a 30% increase in the shrinkage strain is applied in accordance with EN 1992-1-1 Section 3.1.4(6) (SIS – Swedish Institute for Standards, 2005).

The crack width verification is performed in accordance with Eurocode 2, Section 7.3.4 (SIS – Swedish Institute for Standards, 2005). The characteristic crack width is calculated as:

$$w_k = s_{r,max}(\varepsilon_{sm} - \varepsilon_{cm}) \tag{6.4}$$

where $s_{r,max}$ is the maximum crack spacing and $\varepsilon_{sm} - \varepsilon_{cm}$ is the difference between the mean strain in the reinforcement and the mean strain in the concrete between cracks, calculated as:

$$\varepsilon_{sm} - \varepsilon_{cm} = \varepsilon_{cs} - k_t \frac{f_{ct,eff}}{E_s \rho_{p,eff}}(1 + \alpha_e \rho_{p,eff}) \geq 0{,}6 \frac{\sigma_s}{E_s} \tag{6.5}$$

where ε_{cs} is the total shrinkage strain, k_t is a factor accounting for the duration of loading, $f_{ct,eff}$ is the effective tensile strength of the concrete, E_s is the elastic modulus of the reinforcement steel, $\rho_{p,eff}$ is the effective reinforcement ratio, and $\alpha_e = E_s/E_{cm}$ is the modular ratio. The maximum crack spacing is calculated as:

$$s_{r,max} = k_3 c + k_1 k_2 k_4 \frac{\phi}{\rho_{p,eff}} \tag{6.6}$$

where c is the concrete cover, ϕ is the bar diameter, and k_1, k_2, k_3 and k_4 are coefficients. The values adopted in this study are summarised in Table 6.12.

Table 6.12: Parameters used in the crack width calculation.

Parameter	Value	Description
c	30 mm	Concrete cover
ϕ	12 mm	Bar diameter
k_1	0.8	Bond coefficient (ribbed bars)
k_2	1.0	Strain distribution (pure tension)
k_3	2.8	Coefficient per EKS12
k_4	0.425	Coefficient per EN 1992-1-1 Section 7.3.4(3)
k_t	0.4	Long-term loading factor
E_s	200 GPa	Elastic modulus of reinforcement

Since both elements are in contact with soil and subject to moisture, limiting crack widths is essential to reduce the risk of water ingress. A conservative maximum allowable crack width of $w_{max} = 0{,}2$ mm is therefore adopted.

The required reinforcement is determined in two steps. First, the minimum crack-distributing reinforcement is calculated in accordance with EC2 Section 7.3.2, which yields a minimum bar spacing s. This spacing is then used as the centre-to-centre distance between bars, from which the corresponding reinforcement area is derived. The resulting reinforcement area is subsequently verified against the crack width limit. The calculations were performed in Excel and the template is provided in Appendix D.

The results for each strength class are presented in Table 6.13. For all investigated strength classes except C20/25, the crack width criterion is satisfied when the bar spacing derived from the minimum reinforcement requirement is adopted. For C20/25, the resulting crack width exceeds $w_{max} = 0{,}2$ mm, and a reduced bar spacing of $s = 190$ mm is required to satisfy the criterion.

Table 6.13: Required reinforcement for crack width control for the ground slab and basement wall. For C20/25, a reduced bar spacing is required to satisfy $w_{max} = 0{,}2$ mm.

Concrete class	s_{ber} [mm]	A_s [mm^2/m]	w_k [mm]
C20/25	229 (190*)	494 (595*)	0.24 (0.20*)
C25/30	194	583	0.20
C28/35	180	628	0.19
C30/37	174	650	0.18
C32/40	168	673	0.17
C35/45	158	716	0.16
C40/50	144	785	0.15

* Values obtained using a reduced bar spacing of $s_{ber} = 190$ mm.

The results show that the required reinforcement for crack width control increases consistently with increasing concrete strength class, ranging from 583 mm^2/m for C25/30 to 785 mm^2/m for C40/50, with an average increase of approximately 7–8% per strength class step. The trend reflects the direct dependence of the minimum reinforcement requirement on f_{ctm}, which increases with the concrete strength class.

6.7 Environmental Impact

6.7.1 The Impact of the Concrete Elements

To quantify the environmental impact of the structural concrete, the relevant volumes are estimated based on the drawing quantities and assumed cross-sectional dimensions. Three structural elements are considered: the floor slab, the basement external wall, and the ground floor slab. The calculated volumes are summarised in Table 6.14.

Table 6.14: Estimated concrete volumes for the investigated structural elements.

Element	Area [m^2]	Thickness [m]	Volume [m^3]
Floor slab (BJL01)	11 346	0.20	2 269
Basement external wall (YVK01)	604	0.25	151
Ground slab (GVB01–03)	408	0.25	102
Total			**2 522**

The floor slab area corresponds to the in-situ concrete topping only, excluding the prefabricated filigree element. The basement external wall area is taken as the total wall area of 604 m^2, and the ground floor slab covers an area of 408 m^2.

The climate impact of the investigated concrete elements is evaluated using the emission values published by Svensk Betong for factory-mixed concrete, summarised in Table 2.5. The values are expressed as net emissions in kg CO_2-eq./m^3, which are used here as the main basis for comparison.

It should be noted that the exact climate reduction level of the investigated concretes is not known. The available information concerns the slag content of the mixes, while the final classification into one of Svensk Betong's climate performance levels depends on several parameters in addition to the binder composition. The investigated concretes are therefore assumed to correspond approximately to either Level 3 or Level 4, while the industry reference is included as a baseline for comparison.

To assign representative emission values, each structural element is matched to the most relevant category in Table 2.5 based on its exposure conditions. The floor slab is treated as an indoor element in a dry environment and is therefore associated with Category 2 (X0/XC1). The ground slab is associated with Category 3, corresponding to frost-free ground structures below the groundwater level. The basement external wall does not correspond directly to a single tabulated case. Since the wall is partly protected by insulation and partly separated from the surrounding soil by a drainage layer, it is approximated using the Category 3 case for non-frost-free structures above or below the groundwater level. This is considered a conservative assumption.

For the basement wall category, emission values are explicitly tabulated only for C28/35. The corresponding values for C30/37 are therefore estimated based on the difference between the two strength classes in the most comparable tabulated category. These estimated values are used only to enable a consistent comparison between C30/37 and C28/35 and should not be interpreted as official tabulated values.

The resulting CO_2 emissions for each element and performance level are presented in Tables 6.15 and 6.16 for C30/37 and C28/35 respectively.

Table 6.15: Total CO_2-equivalent emissions [tonnes] for C30/37 across structural elements and performance levels.

	Industry reference		**Level 3**		**Level 4**	
Element	**kg/m^3**	**tonnes**	**kg/m^3**	**tonnes**	**kg/m^3**	**tonnes**
Floor slab	230	522	160	363	135	306
Ground floor slab	230	23	160	16	135	14
Basement ext. wall	260*	39	180*	27	150*	23
Total		**584**		**406**		**343**

* Estimated value, not directly tabulated for this exposure class.

Table 6.16: Total CO_2-equivalent emissions [tonnes] for C28/35 across structural elements and performance levels.

Element	Industry reference		Level 3		Level 4	
	kg/m^3	tonnes	kg/m^3	tonnes	kg/m^3	tonnes
Floor slab	215	488	150	340	130	295
Ground floor slab	215	22	150	15	130	13
Basement ext. wall	245	37	170	26	145	22
Total		**547**		**381**		**330**

The total CO_2-equivalent emissions amounted to 406 tonnes for C30/37 and 381 tonnes for C28/35 at Level 3, corresponding to a reduction of 25 tonnes. At Level 4, the corresponding values were 343 tonnes and 330 tonnes, respectively, corresponding to a reduction of 13 tonnes.

Table 6.17: Comparison of total CO_2-equivalent emissions for C30/37 and C28/35 at Level 3 and Level 4.

Performance level	Difference [tonnes]	Reduction [%]
Level 3	25	6.2
Level 4	13	3.8

If the delayed strength development of slag-containing concrete can be utilised in design, it may be possible to reduce the specified strength class from C30/37 to C28/35. The corresponding reduction in total CO_2-equivalent emissions is shown in Table 6.17 for performance Levels 3 and 4.

It can be seen that such a reduction in strength class would decrease the total emissions by approximately 25 tonnes at Level 3 and 13 tonnes at Level 4. This corresponds to a reduction of about 6.2% and 3.8%, respectively.

The results therefore indicate that, if the later-age strength development of slag-based concrete can be structurally utilised, a lower specified strength class may lead to a measurable reduction in embodied carbon.

6.7.2 Reinforcement Volumes — Ground Slab and Basement Wall

A reduction in concrete strength class may, depending on the structural element and the governing design criterion, lead to changes in reinforcement demand. As established in the previous section, the reinforcement demand for the ground slab and basement wall is governed by crack width control, which is directly dependent on the concrete strength class.

A central aspect of this study is that C28/35 with 32% GGBS is assumed to reach the 56-day compressive strength corresponding to C30/37. If this later-age strength is used as the basis for design, the structural element must still be reinforced according to C30/37, since it is the strength class the element is expected to perform as. Specifying C28/35 while reinforcing for C28/35 would therefore constitute under-reinforcement relative to the intended performance level. Consequently, no reinforcement savings are achieved when utilising the later-age strength development, the climate benefit is derived exclusively from the reduced binder content of the concrete itself.

Ground Slab

To illustrate the consequences of overlooking this requirement, Table 6.18 presents the reinforcement quantities and associated CO_2-equivalent emissions for C28/35 and C30/37 for the ground slab. The reinforcement demand is based on the crack width results presented in Table 6.13, and the total quantity is estimated over the full slab area of 408 m^2, assuming uniform distribution in both orthogonal directions:

$$V_s = 2 \cdot A_s \cdot A \cdot 10^{-6}, \tag{6.7}$$

where A_s is the required reinforcement area in mm^2/m, A is the slab area in m^2, the factor 2 accounts for reinforcement in two directions, and 10^{-6} converts mm^2 to m^2. The reinforcement mass was then calculated as

$$m_s = V_s \rho_s, \tag{6.8}$$

where the density of reinforcement steel was taken as $\rho_s = 7800$ kg/m^3. The reinforcement climate impact was calculated using 373 kg CO_2-eq./tonne, corresponding to modules A1–A3 for Swedish reinforcement steel based on the EPD from 7 Steel Service Sweden AB (7 Steel Service Sweden AB, 2025). Reinforcement steel used in Sweden is today produced to a very large extent from recycled material, and the selected EPD value is therefore considered representative of current industry practice (Skanska, 2023).

Table 6.18: Estimated reinforcement quantities and associated climate impact for the ground slab for C28/35 and C30/37.

Concrete strength class	A_s [mm^2/m]	Steel mass [kg]	CO_2-eq. [kg]
C28/35	628	3997	1491
C30/37	650	4137	1543
Difference	22	140	52

The results show that if C28/35 is incorrectly reinforced according to its own strength class rather than C30/37, the reinforcement saving amounts to only 140 kg, corresponding to approximately 52 kg CO_2-equivalent. While this difference is small, it represents an under-reinforcement relative to the intended performance level and should not be treated as a design saving. When utilising the later-age strength of C28/35 to achieve C30/37 performance, the reinforcement must be specified according to C30/37, and no reinforcement-related climate benefit should be claimed.

Basement Walls

Since the horizontal reinforcement demand is assumed to follow the same principles as the ground slab, the change in reinforcement requirement per concrete strength class presented in Table 6.13 is applicable here as well. The total basement wall area was determined to be 604 m^2 as presented in Table 6.14. The wall height varies along the building, and a representative value of 2.7 m is therefore adopted, giving a total wall length of approximately 224 m.

Following the same approach as in the previous section, the total reinforcement volume is estimated as:

$$V_s = A_s \cdot L \cdot 10^{-6}, \tag{6.9}$$

where A_s is the required horizontal reinforcement area in mm^2/m and L is the total wall length in m. Note that the factor of 2 for two reinforcement layers is not applied here, as the values in Table 6.13 already represent the total reinforcement area for a double-reinforced cross-section. The reinforcement mass is then calculated as:

$$m_s = V_s \rho_s, \tag{6.10}$$

where $\rho_s = 7800$ kg/m^3. The reinforcement climate impact was calculated using 373 kg CO_2-eq./tonne in accordance with the EPD from 7 Steel Service Sweden AB (7 Steel Service Sweden AB, 2025).

Table 6.19: Estimated reinforcement quantities and associated climate impact for the basement wall for C28/35 and C30/37.

Concrete strength class	A_s [mm^2/m]	Steel mass [kg]	CO_2-eq. [kg]
C28/35	628	1097	409
C30/37	650	1136	424
Difference	22	39	15

As for the ground slab, the difference in reinforcement demand between C28/35 and C30/37 is small, amounting to approximately 39 kg of steel and 15 kg CO_2-equivalent. It should again be emphasised that if C28/35 is used with the intention of achieving C30/37 performance at 56 days, the reinforcement must be specified according to C30/37. The values for C28/35 are therefore presented only to illustrate the consequence of incorrectly reinforcing for the lower strength class.

7 Discussion

The results presented in this study cover several aspects of climate-reduced concrete, ranging from early-age strength development and long-term hardening to reinforcement demand, deflection behaviour, and embodied carbon emissions. This chapter synthesises the key findings across these areas and discusses their broader implications for structural design practice.

Long-Term Strength Development of GGBS Concrete

A central finding of this study is that concrete containing 32% GGBS consistently exhibits a more pronounced strength gain between 28 and 56 days compared to conventional Portland cement concrete. As shown in the PPB simulations presented in Chapter 5, strength increases of approximately 9–15% were observed over this period for the slag-containing mixes, compared to 3–4% for the Portland reference. This behaviour was consistent across all three investigated structural elements and aligns with the theoretical background discussed in Section 2.2.1, where the delayed pozzolanic reactions of GGBS were identified as the primary driver of continued long-term strength development.

Of particular relevance to the research question is the finding that C28/35 with 32% GGBS continues to develop strength significantly beyond 28 days and, under the simulated conditions, may approach or eventually reach the 37 MPa cube strength associated with C30/37 at a later age. However, the results indicate that this does not necessarily occur as early as 56 days. In the investigated case, the simulated strength development suggests that approximately 80 days were required for the ground slab concrete to reach this level. The 56-day strength should therefore not be interpreted as a universal threshold, but rather as an important intermediate stage in the continued strength development of slag-containing concrete.

This supports the hypothesis that a lower specified strength class may be structurally justified if the later-age strength development of slag-based concrete is accounted for in design. At the same time, the results show that the relevant design age may need to extend beyond 56 days depending on the structural element and the prevailing curing conditions. It should also be noted that the simulations are based on a specific set of boundary conditions, including a spring temperature history in Gothenburg and a fixed GGBS replacement level of 32%. As discussed in Section 2.3, the early-age strength development of slag-containing concretes is particularly sensitive to temperature, and the results may differ significantly under colder curing conditions.

Discrepancy Between Laboratory Results and PPB Simulations

The comparison between PPB predictions and laboratory measurements, presented in Section 4.6, reveals a systematic underestimation of the strength gain between 28 and 56 days. While PPB consistently predicts an increase of approximately 5–6%, the laboratory results show a wider range of approximately 3–13%, with an average of around 8%. The largest discrepancies occur for mixes with higher GGBS contents, which is expected given that the model was calibrated against a concrete with approximately 32% GGBS.

From a design perspective, this conservatism is not necessarily problematic, as it implies that the actual strength development in the field is likely to exceed what the model predicts. However, it also highlights a fundamental limitation of the modelling approach, since PPB does not allow the GGBS content to be explicitly varied as a single parameter, the influence of slag content on later-age strength development is only captured indirectly through the calibrated material model. A more accurate representation would require mix-specific calibration data, which was not available within the scope of this study.

Furthermore, the laboratory results themselves exhibit considerable scatter between mixes of nominally the same strength class, as seen in Table 4.7. This variability underlines the difficulty of establishing general predictive models for climate-reduced concrete and suggests that any practical application of later-age strength in design would need to be supported by mix-specific testing.

Reinforcement Demand and the Role of Concrete Strength Class

The parametric study presented in Section 6.5 demonstrates that the concrete strength class has only a minor influence on the reinforcement required to satisfy ULS bending. The required reinforcement area varies by less than 6% between C25/30 and C40/50 across all investigated spans, reflecting the fact that flexural capacity in ULS is primarily governed by the tensile reinforcement rather than the concrete compressive strength.

In contrast, the minimum reinforcement for crack width control increases with the concrete strength class. For shorter spans, where the ULS demand is closer to the minimum reinforcement level, a reduction in strength class therefore results in a lower minimum reinforcement requirement. For longer spans, where ULS bending governs, the reinforcement demand is largely independent of the strength class, and the climate benefit of a lower class is not counteracted by any significant increase in reinforcement demand.

When crack width is the governing criterion, the required reinforcement is more sensitive to the exposure class and the allowable crack width limit than to the concrete strength class itself. As shown in Section 6.6, the difference in required reinforcement area between adjacent strength classes is small, typically on the order of 20–30 mm^2/m. In practice, reinforcement is commonly specified using standardised welded mesh fabrics with fixed bar spacings, meaning that the actual reinforcement provided is rounded up to the nearest available mesh type. The marginal difference in required reinforcement between adjacent strength classes will therefore rarely translate into a change in the selected mesh, and the practical influence of strength class on reinforcement demand is in most cases negligible when crack width governs.

For the ground slab and basement wall, where crack width control is the governing criterion, the difference in required reinforcement between C28/35 and C30/37 amounts to 22 mm^2/m. If the later-age strength development of C28/35 is accounted for in design, that is, if the element is expected to eventually perform as C30/37, the reinforcement should strictly be specified according to C30/37. Designing for C28/35 while the concrete in reality reaches C30/37 performance at a later age therefore implies a marginal under-reinforcement relative to the actual long-term behaviour of the element.

In practice, reinforcement for ground slabs and basement walls is commonly selected from standardised welded mesh fabrics with fixed bar spacings, meaning that the reinforcement area is rounded up to the nearest available mesh type. Whether this under-reinforcement has any practical consequence therefore depends on whether the 22 mm^2/m difference causes a shift to a mesh with a larger bar spacing. In most cases it will not, and the selected mesh will satisfy the C30/37 crack width criterion regardless. However, in borderline cases where the C28/35 requirement falls just below a mesh boundary, the chosen mesh may be too coarse to satisfy the crack width limit corresponding to the concrete's actual long-term strength class. This represents a practical consideration that should be kept in mind when utilising later-age strength in design.

Production Implications of Delayed Early-Age Strength

While the long-term strength development of GGBS concrete is advantageous from a structural and environmental perspective, the slower early-age strength gain has direct consequences for the construction process. As shown in Table 5.3, the time required to reach 5 MPa, which governs the earliest possible formwork removal for the basement wall, is approximately twice as long for the slag-containing concretes compared to the Portland reference. Similarly, the time to reach 35% of $f_{ck,cube}$, which determines the end of the required curing period in accordance with curing class 2, is approximately 40–43 hours for the GGBS mixes compared to 17 hours for Portland.

These delays are likely to affect the construction tact, particularly for basement walls and other elements where formwork removal is on the critical path of the production schedule. As discussed in Section 2.7.1, a mismatch between the planned tact and the actual hardening rate can either force premature loading or cause delays that propagate through subsequent construction stages. The trade-off between reduced embodied carbon and potential increases in construction time therefore represents an important practical consideration when specifying climate-reduced concrete for elements with tight production cycles.

Climate Impact: Strength Class Versus Performance Level

The environmental analysis presented in Section 5.5.2 demonstrates that the choice of climate performance level has a substantially larger influence on the total embodied carbon than the choice of concrete strength class. Moving from the industry reference to Level 3 reduces total emissions by approximately 30%, while the difference between C30/37 and C28/35 at the same performance level amounts to approximately 6% at Level 3 and 4% at Level 4.

This suggests that the primary lever for reducing embodied carbon is the selection of a climate-optimised mix, rather than the specific strength class. Nevertheless, the additional reduction achievable through a lower strength class, approximately 25 tonnes of CO_2-equivalent at Level 3 for the investigated building, is not negligible and represents a meaningful contribution when considered across multiple projects or at a larger scale.

The relatively small influence of strength class on embodied carbon also has implications in the opposite direction. Since increasing the strength class by one step incurs only a marginal increase in emissions, it may in some cases be advantageous to specify a higher strength class in combination with a highly climate-optimised mix. A higher strength class would partially counteract the slower early-age strength development associated with high supplementary cementitious material contents, while the emissions penalty of the upward class shift remains small relative to the savings achieved through the climate-optimised binder composition. This trade-off warrants consideration in practical mix selection, particularly for elements where early-age strength is critical for the construction schedule.

Limitations and Uncertainties

Several limitations of the present study should be acknowledged. The PPB calibration was performed against a single concrete mix with approximately 32% GGBS, and the calibrated material model was subsequently applied to mixes with different binder compositions without further adjustment. As shown in Section 4.6, this leads to underestimation of the later-age strength gain for mixes with higher slag contents.

The structural analyses were performed on a simplified unit strip model assuming simply supported boundary conditions, as described in Section 5.6. Real floor slabs typically exhibit two-way action and partial continuity, which would affect both the reinforcement demand and the deflection response. The results should therefore be regarded as indicative rather than directly applicable to specific design situations.

8 Conclusion

8.1 Main conclusions

This study investigated the structural and environmental implications of using climate-reduced concrete with ground granulated blast-furnace slag (GGBS) as a partial cement replacement, with a particular focus on whether later-age strength development can justify the use of lower concrete strength classes in design.

The results of this study indicate that climate-reduced concrete with GGBS exhibits continued strength development beyond 28 days, often reaching significantly higher compressive strengths at later ages. This suggests that the conventional use of 28-day strength as the governing design parameter may, in some cases, lead to an underutilisation of the material's long-term capacity.

By instead considering 56-day strength as a basis for design, it may be possible to utilise lower strength classes while still achieving the required performance at later ages. This approach has the potential to reduce material use, particularly cement content, and thereby contribute to lower CO_2 emissions, with a one-class reduction at the same performance level corresponding to an additional carbon reduction of approximately 4–6%.

However, the results also highlight that such an approach cannot be applied without careful consideration. While sufficient strength may be achieved in the long term, the slower early-age strength development associated with GGBS concrete introduces challenges related to construction processes and structural performance during the initial stages. Factors such as formwork removal, load application, and temperature conditions during curing must be evaluated in detail.

Furthermore, the variability observed in strength development between different concrete mixes indicates that reliable prediction methods are required to ensure safe and efficient design. Before adopting later-age strength as a general design principle, a comprehensive assessment of both short-term and long-term behaviour is necessary.

In conclusion, the findings demonstrate a clear potential for more efficient utilisation of climate-reduced concrete, but also emphasise the need for a holistic approach that accounts for both early-age behaviour and long-term performance.

8.2 Further Research

Based on the findings of this study, several areas have been identified where further research would be valuable:

- **Early-age behaviour, mitigation strategies, and cost–climate trade-offs:** Further research should investigate the early-age strength development (1–7 days) of GGBS concrete under varying temperature conditions, with particular focus on how curing temperature, binder composition, and mix design influence the rate of strength gain. This should be directly linked to the identification of practical measures required to ensure sufficient early strength, such as adjustments in mix composition, use of accelerators, or modified curing procedures. In addition, the economic implications of these measures should be quantified, including their impact on construction time, formwork removal, and overall production efficiency. A comprehensive evaluation should also compare these additional costs with the achieved reductions in CO_2 emissions, in order to identify solutions that are both economically and environmentally optimal.

- **Long-term strength development and identification of strength plateau:** Comprehensive experimental programmes with extended laboratory testing (e.g. up to 56, 90 days or longer) are needed to better characterise the long-term strength development of GGBS concrete. Such studies should include a wide range of mix compositions to capture variability and improve the reliability of observed trends. Particular emphasis should be placed on identifying when the strength development begins to level off, and how this behaviour depends on binder composition, curing conditions, and temperature history. The results could provide a more robust basis for design assumptions beyond 28 days.

9 References

7 Steel Service Sweden AB. (2025, July). Environmental product declaration: Steel reinforcement products for concrete – swedish production from 7 steel service sweden ab [EPD registration number: S-P-00305, valid until 2026-09-29].

Al-Emrani, M., Engström, B., Johansson, M., & Johansson, P. (2019). *Bärande konstruktioner*. Chalmers University of Technology.

ASTM C1074-19e1. (2019). *Standard practice for estimating concrete strength by the maturity method* [Editorially corrected January 2021]. ASTM International. West Conshohocken, PA. https://doi.org/10.1520/C1074-19E01

Bokelid, G., & Fayed, K. (2022). *Taktplanering i byggnadsprojekt - fördelar och nackdelar* [Master's Thesis]. Lund University, Faculty of Engineering (LTH).

Buitrago, M., Sagaseta, J., & Adam, J. M. (2020). Avoiding failures during building construction using structural fuses as load limiters on temporary shoring structures. *Engineering Structures*, *204*, 109906. https://doi.org/10.1016/j.engstruct.2019.109906

Doka GmbH. (2020). *Shoring and reshoring of concrete slabs*. Doka GmbH.

Doka GmbH. (2024, March). *Stämp eurex 20 lw: Användarinformation* [Dokumentnr. 999816010 03/2024 sv]. Doka GmbH. Amstetten, Österrike.

Engström, B. (2014). *Restraint cracking of reinforced concrete structures* (Technical Report No. Report 2007:10, Edition 2014). Chalmers University of Technology, Department of Civil and Environmental Engineering, Division of Structural Engineering. Göteborg, Sweden.

Formmax AB. (2014, November). *Monteringsstöd: Användningsriktlinjer* [Teknisk broschyr för Hünnebecks monteringsstöd]. Örebro, Sweden.

Hafiz, M. A., Skibsted, J., & Denarié, E. (2020). Influence of low curing temperatures on the tensile response of low clinker strain hardening uhpfrc under full restraint. *Cement and Concrete Research*, *128*, 105940. https://doi.org/10.1016/j.cemconres.2019.105940

Hedlund, H., Westman, B., & Groth, P. (1996). *Känslighetsanalys spänningsberäkning – monte carlo simulering för normalpresterande betong* (Research report No. Skrift 96:02). Luleå tekniska universitet, Avdelningen för Konstruktionsteknik.

Hilti Group. (2024). *On-site testing of fastenings in concrete* [Accessed 2026-01-21]. https://www.hilti.se/content/hilti/E1/SE/sv/business/business/engineering/onsite-testing.html

Jeremi, L. O., Mohammed, B. S., Al-Yacouby, A. M., & Abbas, F. O. (2026). Optimizing sustainability in cement production: A combined lca and topsis approach for evaluating ggbs substitution and alternative energy strategies. *Carbon Management*, *17*(1), 2610583. https://doi.org/10.1080/17583004.2025.2610583

Johnsson, A. (2017). *Verkliga kostnader för bostadsbyggandet: Begrepp och kostnadsfördelning [real costs for housing construction: Concepts and cost distribution]* (tech. rep. No. 12666) (In Swedish). Svenska Byggbranschens Utvecklingsfond (SBUF). Gothenburg, Sweden.

Konietzky, H. (2020). *Concrete for geotechnical engineering* [updated November 2020]. TU Bergakademie Freiberg.

Kurdowski, W. (2014). *Cement and concrete chemistry*. Springer. https://doi.org/10.1007/978-94-007-7945-7

Lättklinkerbetong AB. (2020). *Montagehandbok: Sandwichvägg • massivvägg* [Technical manual for prefabricated concrete elements]. Umeå, Sweden.

Ljungkrantz, C., Möller, G., & Petersons, N. (Eds.). (1992). *Betonghandbok: Arbetsutförande—projektering och byggande* [Tryck: Ljungföretagen Örebro AB. Illustrationer: Piroska von Gegerfelt]. Svensk Byggtjänst; Cementa AB.

Ljungkrantz, C., Möller, G., & Petersons, N. (Eds.). (1994). *Betonghandboken material* (2nd ed.). Svensk Byggtjänst; Cementa AB.

Magnusson, J., Mathern, A., Saleh, I., Löfgren, I., Berrocal, C. G., Suchorzewski, J., & Rempling, R. (2024). *Metoder för sprickriskbedömning och -begränsning hos hårdnande betong: En omvärldsanalys och parameterstudie* (Technical Report No. Project No. 14170). Svenska Byggbranschens Utvecklingsfond (SBUF). Stockholm, Sweden.

Olsson, A. (2019). *Modellering av tidig rivning av bärande form och stämpborttagning* [Master's thesis, Luleå tekniska universitet].

Oner, A., & Akyuz, S. (2007). An experimental study on optimum usage of GGBS for the compressive strength of concrete. *Cement & Concrete Composites*, *29*, 505–514. https://doi.org/10.1016/j.cemconcomp.2007.01.001

Osman, J. (2020). *Dimensionering av filigranbjälklag med fem-design* [Examensarbete]. Luleå tekniska universitet, Institutionen för samhällsbyggnad och naturresurser [Examensarbete, Civilingenjör Väg- och vattenbyggnad, i samarbete med Skanska Sverige AB].

Pettersson, M., & Strömberg, P. (2013). *Utfackningsväggar: En jämförelse mellan platsbyggda och prefabricerade byggmetoder* [Degree Project in Civil Engineering]. Uppsala University, Department of Engineering Sciences.

Ramezanianpour, A. A. (2014). *Cement replacement materials: Properties, durability, sustainability*. Springer Heidelberg. https://doi.org/10.1007/978-3-642-36721-2

Schake GmbH. (2024). Slanted prop v11. https://www.schake.com/en/products/construction-equipment-traffic-safety/formwork/slanted-prop/v11.html

SIS – Swedish Institute for Standards. (2005). *Ss-en 1992-1-1:2005 (sv): Eurokod 2 – dimensionering av betongkonstruktioner – del 1-1: Allmänna regler och regler för byggnader*.

SIS – Swedish Institute for Standards. (2009). *Ss-en 13670:2009: Execution of concrete structures*.

SIS – Swedish Institute for Standards. (2025). *Ss 137003:2021+t2:2025: Betong – användning av SS-EN 206:2013+a2:2021 i Sverige*.

SIS – Swedish Standards Institute. (2015, maj). *Betongkonstruktioner – utförande – tillämpning av ss-en 13670:2009 i sverige* (Svensk Standard No. SS 137006:2015) (Utgåva 2). SIS, Swedish Standards Institute. Stockholm, Sverige.

Skandinaviska Byggelement AB. (2016). *Montagehandbok: Skalvägg • plattbärlag* [Technical manual for pre-cast concrete shell walls and filigree slabs]. Katrineholm, Sweden.

Skanska. (2023). Armering med lågt klimatavtryck hjälper solna link nå målen [Accessed: 2026-05-04]. https://www.skanska.se/om-skanska/press/nyheter/armering-med-lagt-klimatavtryck-hjalper-solna-link-na-malen/

SMHI. (2026). Air temperature observations, station 71420 [Accessed: 2026-03-17]. https://www.smhi.se/data/hitta-data-for-en-plats/ladda-ner-vaderobservationer/airtemperatureInstant/71420

Soutsos, M., & Domone, P. (Eds.). (2018). *Construction materials: Their nature and behaviour* (5th ed.). CRC Press.

Sundelius, P., & Wahlqvist, E. (2022). *The risk of early-age thermal cracking using concrete with high ggbs content: A parametric study of two concrete mixes for a wall-to-slab section* [Master's thesis]. Chalmers University of Technology, Department of Architecture and Civil Engineering.

Surapha, W., & Sutheerawatthana, P. (2024). Factors in deciding to speed up construction work are schedule cost and CO2 emissions. *Journal of Engineering*, *2024*, 9954310. https://doi.org/10.1155/je/9954310

Svensk Betong. (2025). Bilaga 1 fabriksbetong – vägledning klimatförbättrad betong, utgåva 2 [Updated tables July 2025].

Svensk Byggtjänst. (2023). *AMA anläggning 23*.

Svenska Betongföreningen. (2009). *Vägledning för val av exponeringsklass enligt SS-EN 206-1* (2nd ed., tech. rep. No. 11). Svenska Betongföreningen.

Svenska Byggbranschens Utvecklingsfond. (n.d.). Produktionsplanering betong – branschgemensamt verktyg för planering av betonggjutningar [Available from SBUF].

Thomas Betong AB. (2016). *Montagehandbok: Plattbärlag och skalväggar* [Hämtad från Thomas Betongs dokumentkatalog]. Thomas Betong AB. Göteborg. https://thomasbetong.se

Wang, J., Tingley, D. D., Mayfield, M., & Wang, Y. (2018). Life cycle impact comparison of different concrete floor slabs considering uncertainty and sensitivity analysis. *Journal of Cleaner Production*, *189*, 374–385. https://doi.org/10.1016/j.jclepro.2018.04.094

Zhou, Z., Zhu, H., Wang, M., Wu, Q., Yin, Z., & Ding, H. (2026). Synergistic alkali activation of cement kiln dust and ground granulated blast furnace slag: Material performance and reaction kinetics. *Environmental Research*, *291*, 123564. https://doi.org/10.1016/j.envres.2025.123564

Appendix A

.1 StruSoft output for 5 m span

This appendix presents representative output from the StruSoft analysis for a beam with a span length of 5 m. The figures are provided for documentation and transparency of the numerical modelling and reinforcement design, and serve as a reference for the results discussed in the main text.

Figure .1 shows the structural model used in StruSoft, including geometry, support conditions, and applied loads. Figure .2 presents the elastic bending moment and shear force diagrams obtained from the linear elastic analysis under ULS loading. Figure .3 shows the corresponding reinforcement layout and required reinforcement area resulting from the ULS bending verification.

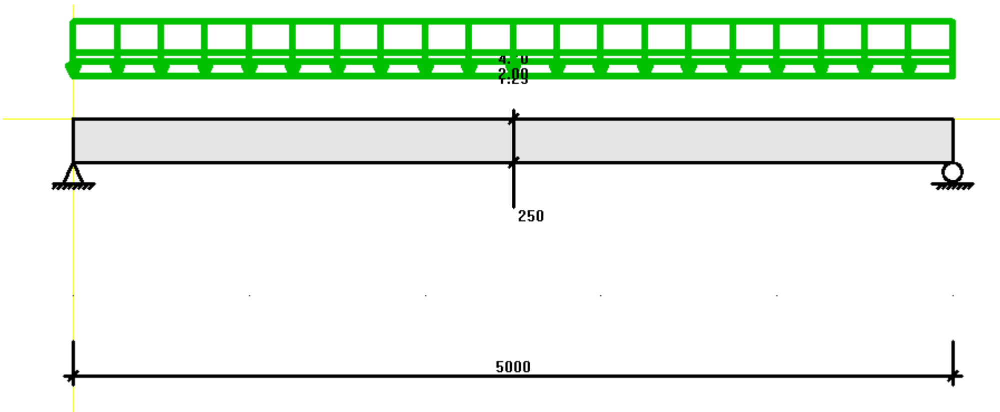

Figure .1: Structural model used in StruSoft for the analysis of a simply supported beam with a span of 5 m, showing geometry, support conditions, and applied loads.

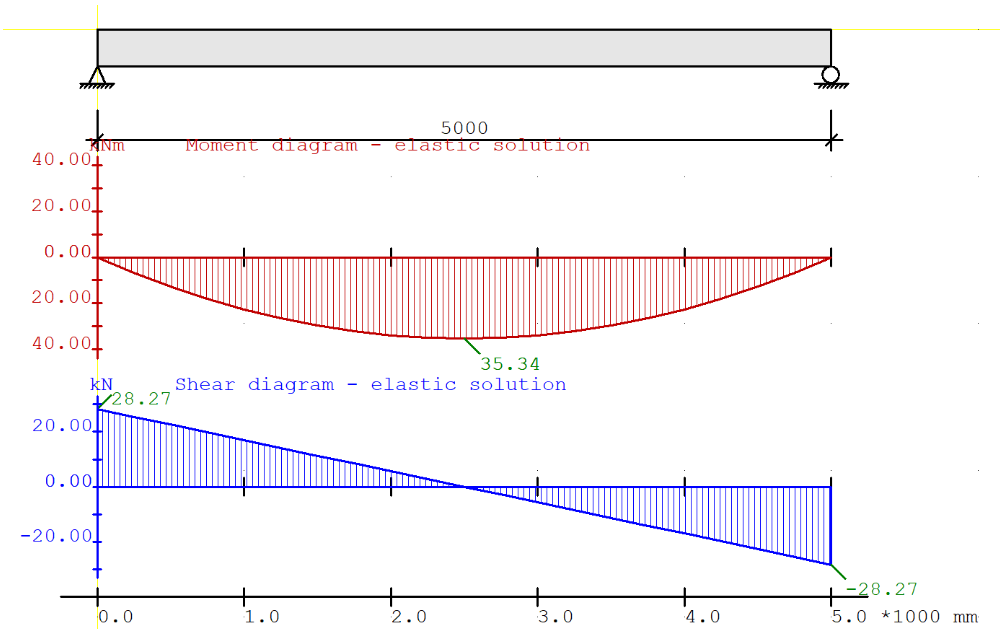

Figure .2: Elastic bending moment and shear force diagrams obtained from the StruSoft analysis for a simply supported beam with a span of 5 m under ULS loading.

Reinforcement due to bending (elastic result)

	L supp.	L supp.	Middle	Middle	R supp.	R supp.
	Bottom	Top	Bottom	Top	Bottom	Top
Span 1						
Reinforcement	4 Ø12 1L	2 Ø12 1L	4 Ø12 1L	2 Ø12 1L	4 Ø12 1L	2 Ø12 1L
Selected area (mm²)	452	226	452	226	452	226
Req. area (mm²)	35	0	372	0	35	0
Eff. depth (mm)	222	222	222	222	222	222
Min. reinforcement	Yes				Yes	

Figure .3: Required tensile reinforcement due to bending obtained from StruSoft for a 5 m span, based on elastic internal forces and cross-section resistance verification in ULS.

Appendix B

Additional tables from the StruSoft serviceability analysis are presented in this appendix.

The first table presents the long-term deflection results, including creep and shrinkage, for concrete modelled with cement class S (slow), used as an approximation of slag-based concrete.

The second table presents the corresponding long-term deflection results for normal Portland concrete.

Table .1: Long-term deflection including creep and shrinkage for concrete modelled with cement class S (slow), used as an approximation of slag-based concrete.

Concrete strength class	**5 m**	**6 m**	**7 m**	**8 m**	**9 m**	**10 m**
C25/30	3.76	18.59	38.69	62.97	76.80	86.33
C30/37	3.40	7.20	35.32	58.25	75.44	85.48
C35/45	3.07	6.51	30.50	54.70	74.87	85.14
C40/50	2.80	5.96	25.51	49.84	74.75	85.11
$L/250$ [mm]	20	24	28	32	36	40

Table .2: Long-term deflection including creep and shrinkage for normal Portland concrete.

Concrete strength class	**5 m**	**6 m**	**7 m**	**8 m**	**9 m**	**10 m**
C25/30	3.76	19.51	41.89	65.75	75.75	88.49
C30/37	3.47	9.13	37.19	61.00	74.63	87.47
C35/45	3.23	6.90	32.22	57.51	73.28	87.00
C40/50	3.04	6.49	27.21	52.75	73.02	86.00
$L/250$ [mm]	20	24	28	32	36	40

Appendix C

.1.1 Creep and shrinkage

Creep and shrinkage are two fundamental time-dependent deformation mechanisms in concrete, both of which significantly influence stress distribution, crack development, and long-term structural behaviour. Shrinkage occurs independently of external loading and is primarily driven by moisture transport and internal chemical processes, whereas creep develops under sustained stress and results in additional deformation over time (Engström, 2014).

Shrinkage may be divided into drying shrinkage, governed by moisture exchange with the environment, and autogenous shrinkage, which occurs due to internal chemical reactions, particularly in low water–cement ratio concretes. Creep, on the other hand, depends on factors such as stress level, age at loading, and environmental conditions, and plays an important role in stress redistribution and relaxation of restraint-induced stresses (Engström, 2014).

These time-dependent effects are particularly important in serviceability limit state (SLS) design, where they contribute to increased deflections and crack widths over time. In this study, creep and shrinkage are considered in the assessment of long-term deflections of filigree floor slabs.

In order to estimate these effects, StruSoft applies calculation models based on the principles meantioned above. The following equations, implemented in the software, are used to determine the creep and shrinkage parameters.

.1.1.1 Creep

Long term cracks

$$\varphi(t,t_0) = \varphi_0 \cdot \beta_c(t,t_0) \tag{.1}$$

$$\varphi_0 = \varphi_{RH} \cdot \beta(f_{cm}) \cdot \beta(t_0) \tag{.2}$$

$$\varphi_{RH} = 1 + \frac{1 - RH/100}{0{,}1 \cdot h_0^{1/3}} \tag{.3}$$

$$\beta(f_{cm}) = \frac{16{,}8}{\sqrt{f_{cm}}} \tag{.4}$$

$$\beta(t_0) = \frac{1}{0{,}1 + t_0^{0{,}2}} \tag{.5}$$

$$f_{cm} = f_{ck} + 8 \tag{.6}$$

.1.1.2 Shrinkage

Drying shrinkage occurs as moisture evaporates from the concrete over time. The nominal unrestrained drying shrinkage strain is given by:

$$\varepsilon_{cd}(t) = \beta_{ds}(t, t_s) \cdot k_h \cdot \varepsilon_{cd,0} \tag{.7}$$

where $\varepsilon_{cd,0}$ is the nominal unrestrained drying shrinkage, defined as:

$$\varepsilon_{cd,0} = 0{,}85 \cdot \left[(220 + 110 \cdot \alpha_{ds,1}) \cdot e^{-\alpha_{ds,2} \cdot \frac{f_{cm}}{f_{cm0}}}\right] \cdot 10^{-6} \cdot \beta_{RH} \tag{.8}$$

The coefficient β_{RH} accounts for the effect of relative humidity:

$$\beta_{RH} = 1{,}55 \cdot \left[1 - \left(\frac{RH}{100}\right)^3\right] \tag{.9}$$

The coefficient k_h depends on the notional size h_0 and the time-dependent factor $\beta_{ds}(t, t_s)$ is given by:

$$\beta_{ds}(t, t_s) = \frac{(t - t_s)}{(t - t_s) + 0{,}04 \cdot \sqrt{h_0^3}} \tag{.10}$$

where t is the age of concrete in days, t_s is the age of concrete at the beginning of drying shrinkage, and h_0 is the notional size of the cross-section defined as:

$$h_0 = \frac{2A_c}{u} \tag{.11}$$

where A_c is the cross-sectional area and u is the perimeter of the cross-section exposed to drying.

Autogenous Shrinkage Autogenous shrinkage develops during the hydration process, independent of moisture loss, and is particularly relevant in the early stages after casting:

$$\varepsilon_{ca}(t) = \beta_{as}(t) \cdot \varepsilon_{ca,\infty} \tag{.12}$$

where the final autogenous shrinkage strain is:

$$\varepsilon_{ca,\infty} = 2{,}5 \cdot (f_{ck} - 10) \cdot 10^{-6} \tag{.13}$$

and the time function is:

$$\beta_{as}(t) = 1 - e^{-0{,}2\sqrt{t}} \tag{.14}$$

The total shrinkage strain is the sum of drying and autogenous shrinkage:

$$\varepsilon_{cs} = \varepsilon_{cd}(t) + \varepsilon_{ca}(t) \tag{.15}$$

Appendix D

The crack width calculations presented in this study were performed using an Excel template developed for this purpose. The template follows the procedure outlined in Eurocode 2, covering three main steps: determination of shrinkage strains in accordance with EN 1992-1-1 Annex B, calculation of the minimum required crack-distributing reinforcement in accordance with Section 7.3.2, and verification of the characteristic crack width in accordance with Section 7.3.4. The template takes the concrete strength class, relative humidity, cross-section geometry and reinforcement parameters as input, and outputs the required bar spacing, reinforcement area and calculated crack width. A representative output for the basement wall with strength class C20/25 is shown in Figure .4.

Uppdrag	Konstruktionsdel	Utfärdad av
Ex-jobb	Källarvägg (Liggande armering)	Saga
Ort	Datum	
Göteborg	2026-05-06	Indata =

Bestämning av krympning enl. 1992-1-1 Bilaga B

Betongens hållfasthetsklass		C20/25	Tvärsnittets bredd	b [mm] =	1000
Cementklass		1: S	Tvärsnittets höjd	h [mm] =	250
Relativ fuktighet	RH [%]=	55	Yta i kontakt med luft	u [mm] =	1000
Beakta 30% variation?		Ja			
Tvärsnittsarea	A_c [mm^2]=	250000	Tryckhållfasthet	f_{ck} [MPa] =	20
Ekvivalent tjocklek	h_0 [mm]=	500	Tryckhållfasthet, medel	f_{cm} [MPa] =	28
Faktor bektande RH	β_{RH}=	1,29	α-koefficienter	α_{ds1}=	3,00
Uttorkningskrympning	$\varepsilon_{cd,0}$=	4,20E-04		α_{ds2}=	0,13
Koefficient ber. av h_0	k_h=	0,7	Uttorkningskrympning	$\varepsilon_{cd,\infty}$=	2,94E-04
			Autogen krympning	$\varepsilon_{ca,\infty}$=	2,50E-05
Total krympning	$\varepsilon_{cs,\infty}$=	**4,14E-04**			

Bestämning av minsta erfoderliga armering enl. EKS10 och 1992-1-1 7.3.2

Armeringsplacering		Dubbelarmerad	Sträckgräns	f_{yk} [MPa] =	500
Armering		K500B	Draghållfasthet	f_{ctm} [MPa] =	2,2
Armeringsdiameter	Ø [mm]=	12	Koefficient	k=	0,90
Betongyta dragen zon	A_{ct} [mm^2]=	250000	Koefficient	k_c=	1,0

Minsta erfoderliga armering $A_{s,min}$ [mm^2] = 990 s_{ber} [mm]= 229 Fördelad över ÖK och UK

Bestämning av armering med hänsyn till tillåten sprickbredd enligt 1992-1-1 7.3.4

Armering s-avstånd	s [mm]=	190	Effektiv hävarm	d [mm]=	208
Täckskikt	c [mm]=	30	Andel armering/betong	ρ [-] =	5,66E-03
Armeringsmängd	A_s [mm^2]=	595	E-modul armering	E_s [GPa]=	200
Effektiv höjd	$h_{c,ef}$ [mm]=	105	E-modul betong	E_{cm} [GPa]=	30
Effektiv betongyta	$A_{ct,ef}$ [mm^2]=	105000	Kvot	α_e [-] =	6,68
Koefficient	k_1 [-]=	0,8	Koefficient	k_4 [-]=	0,425
Koefficient	k_2 [-]=	1,0	Koefficient	k_t [-]=	0,4
Koefficient	k_3 [-]=	2,8			
Töjningsskillnad	$\varepsilon_{sm}-\varepsilon_{cm}$ =	2,49E-04			
Största sprickavstånd	s_{max} [m]=	0,80			
Sprickbredd	w_k [mm]=	**0,200**			
Vald armering	**#Ø12s190,13**	**Dubbelarmerad ÖK+UK**			

Figure .4: Excel calculations.

DEPARTMENT OF ARCHITECTURE AND
CIVIL ENGINEERING
CHALMERS UNIVERSITY OF TECHNOLOGY
Gothenburg, Sweden 2026
www.chalmers.se

CHALMERS
UNIVERSITY OF TECHNOLOGY